The Function of Toll-like receptor 2 in Infection and Inflammation

Hu, W.

Chapter 4

Specificity of the innate immune responses to different classes of non-tuberculous mycobacteria using a zebrafish larval model

Wanbin Hu, Bjørn Koch, Gabriel Forn-Cuní, Herman P. Spaink

In preparation

4

Abstract

Mycobacterium avium is a slow growing nontuberculous mycobacterium which causes 80% of NTM infectious disease cases worldwide. However, there is neither a straightforward treatment regimen for the disease nor any effective animal models for investigating it. Here, we used zebrafish larvae and took advantage of their transparency and high throughput potential to establish a *M. avium* infectious model. We characterized the *M. avium* MAC 101 infection in larvae comparing it to that of a recognized model of tuberculosis infection, *Mycobacterium marinum* Mma20, in terms of bacterial burden, formation of granuloma-like clusters, gene expression profiles, function of *tlr2* and immune cell migratory behavior. We found that Mma20 is more virulent than MAC 101 in zebrafish larvae. MAC 101 has a distinct transcriptome response compared to Mma20, especially regarding cytokine and chemokines, autophagy regulators, and matrix remodeling. At the cellular level, our results demonstrate that macrophages play an important role in the response to both mycobacterial infections because more recruited macrophages were observed in the infected area. The migration speed of macrophages is faster to Mma20 infection. Interestingly, the MAC 101 infected larvae have a more closed granuloma-like cluster structure, while we observed higher bacterial burden outside macrophages in Mma20 infected larvae. In addition, we found that *tlr2* plays a conservative and protective role for the host upon mycobacterial infection, and is involved in the regulation of the migration of macrophages and neutrophils in response to the infection. Taken together, we characterized a new *M. avium* MAC 101 infection model in zebrafish that can be further used to study the interaction between the host and NTM bacteria.

Introduction

The infectious diseases caused by mycobacterial pathogens other than the *Mycobacterium tuberculosis* (Mtb) and *Mycobacterium leprae* (*M. leprae*) complexes, are collectively called nontuberculous mycobacteria (NTM) infections [1]. NTM include more than 150 species and are ubiquitously distributed in the environment, like soil, dust, and water [2, 3]. Currently, NTM infectious diseases have aroused wide attention because of the rise of its incidences globally [2]. Although there are existing treatments for NTM infectious diseases, the treatment regimens are long and have a high frequency of multi-drug resistant cases [4]. Thus, it is urgent to discover novel prevention and therapeutic strategies for patients infected with NTM. Currently, host-directed therapies (HDT) are one of the most promising strategies to combat NTM infectious diseases by making the NTM antibiotic treatment regimens more effective [5-7]. However, the current knowledge of the mechanisms underlying host-NTM bacteria interactions is limited and therefore more studies are highly needed.

The *Mycobacterium avium complex* (MAC), which consists of the *Mycobacterium intracellulare* (*M. intracellulare*) and *Mycobacterium avium* (*M. avium*) species, is one of the most common disease-causing NTM group [3, 8]. Although MAC bacteria are generally believed to be less virulent for primates than Mtb, they can cause pulmonary and extra-pulmonary disease in susceptible individuals, e.g. patients with acquired immunodeficiency syndrome (AIDS) or with a history of lung disease [9-11]. To be noted, Mtb infected patients can be dually infected with MAC bacteria. Unfortunately, there is no straightforward drug or treatment regime for the MAC infections available [12]. That is, among other reasons, because developing new drugs or treatment regime is challenging due to the limited research and sometimes results are contradictory between *in vitro* and mice *in vivo* studies [13, 14] or between studies using different subspecies of *M. avium*: *M. avium* has four subspecies, and it has been demonstrated that they cause different disease characteristics [15, 16]. A standardized MAC infectious disease animal model is therefore urgently needed to study the mechanism of MAC infection and test new drugs effectively. In previous studies, the *M. avium Chester* (also called MAC 101) infectious capacity has been evaluated in different mouse strains, including BALA/c, C57BL/6, nude, and beige mice, allowing for drug or treatment assessment [17, 18]. Thus, MAC 101 can be considered as a standard strain to investigate *M. avium* infection studies.

Zebrafish (*Danio rerio*) larvae are popular as a model to study human infectious disease because their innate immune system is highly similar to that of mammals and they are optically

accessible making the infectious agents and immune cells easy to track *in vivo* [19]. Furthermore, they enable investigation of innate immune function isolating from adaptive immunity [19-21]. Zebrafish larvae have been an effective model organism to study the mechanism of Mtb infection for over 15 years [22]. A majority of the studies have used *M. marinum* as the infectious agent because it is genetically closely related to Mtb, and has been shown to be the causing granuloma formation in zebrafish larvae at high frequency [23].

Immune cells, as an important part of the innate immune system, depend on pattern recognition receptors (PRRs) to initiate protective innate immune responses in the host [24]. Toll-like receptor 2 (TLR2) serves as one of the most important PRR to sense invaded microbial pathogens through pathogen-associated molecular patterns (PAMPs) [25]. Much progress has been made the last decades in revealing the function of TLR2 in defense against Mtb infection. It has been reported that TLR2 senses invading Mtb bacteria through the lipoproteins and glycolipids located on their cell wall [26, 27]. A profound pro-inflammatory response is triggered after the stimulation of TLR2, which is considered to promote bacterial clearances [28]. However, it has been shown that activation of TLR2 also activates anti-inflammatory responses [29]. The PRR feature of TLR2 makes it popular as a therapeutic target for TB [30]. However, there is little known about the involvement of TLR2 in *M. avium* infection.

In this study, we developed an innovative zebrafish larval infectious model for studying *M. avium* infection. Moreover, we compared the innate immune response of zebrafish larvae to infection with two different species of NTM, *M. marinum* Mma20 and *M. avium* MAC 101, specifically with regard to the bacterial burden, granuloma-like cluster formation, and transcriptomic gene expression profiles. Using this system, we analyzed the function of *tlr2* during the infection with both mycobacterial species with special attention to the responsive cell migration behavior.

Results

M. marinum is more virulent than *M. avium* in zebrafish larvae

To compare the virulence of *M. avium* MAC101 and *M. marinum* Mma20, we infected zebrafish larvae with increasing dosages of the two species of mycobacteria carrying fluorescent protein reporters. We infected the larvae systemically by injection into the caudal vein at 28 hours post fertilization (hpf) and monitored larval survival and infectious

development by fluorescent microscopy over the following 4 days. The representative images for the bacterial burden quantification are shown in Fig. 1A. The results clearly demonstrated that infection with Mma20 was drastically more lethal than with MAC 101 over the 4-day assessment period. Even at the highest infectious dose of 9000 colony forming units (CFU) of MAC101, 86.67% (26/30) of larvae survived until the end of the experiment, and with lower dosages of 4500 and 1000 CFU, the survival was higher than 90% (Fig. 1B). In contrast, 73.33% (22/30) of larvae infected with 500 CFU Mma20 survived until 4 days post infection (dpi) and only 16.13% (5/31) larvae survived in 1000 CFU Mma20 group (Fig. 1B), while the survival rate of the larvae infected with the dose of 250 CFU Mma20 was 96.67% (29/30). We subsequently assessed the infectious development of MAC 101 and Mma20 by microscopy-based analysis, using fluorescent signal derived from the injected bacteria as a proxy for the infectious status in the larvae. Larvae infected with 250 CFU Mma20 and 4500 and 9000 CFU MAC 101 all exhibited significant increases in the fluorescent signal at 4 dpi compared with 1 dpi (Fig. 1C, D and E), indicating a progressing infection despite the low overall mortality in these groups. Interestingly, while the fluorescent signal in Mma20 infected larvae rose steadily from 1 to 4 dpi, MAC 101 infected larvae exhibited a drop in fluorescent signal from 1 to 2 dpi, only to recover and grow at 3 and 4 dpi. This underscores the different dynamics of infection between these two species of mycobacteria. Taken together, these results show that Mma20 causes a more rapid disease development and higher mortality compared to MAC 101 which declines during the first days of the infection, but recovers and may cause mortality at later time points than what we could measure with this experimental setup. Having characterized these broad spanning CFU burdens, moving forward we focused only on two groups: 250 CFU for Mma20 and 4500 CFU for MAC 101, as these have similar mortality and measurable fluorescent signals.

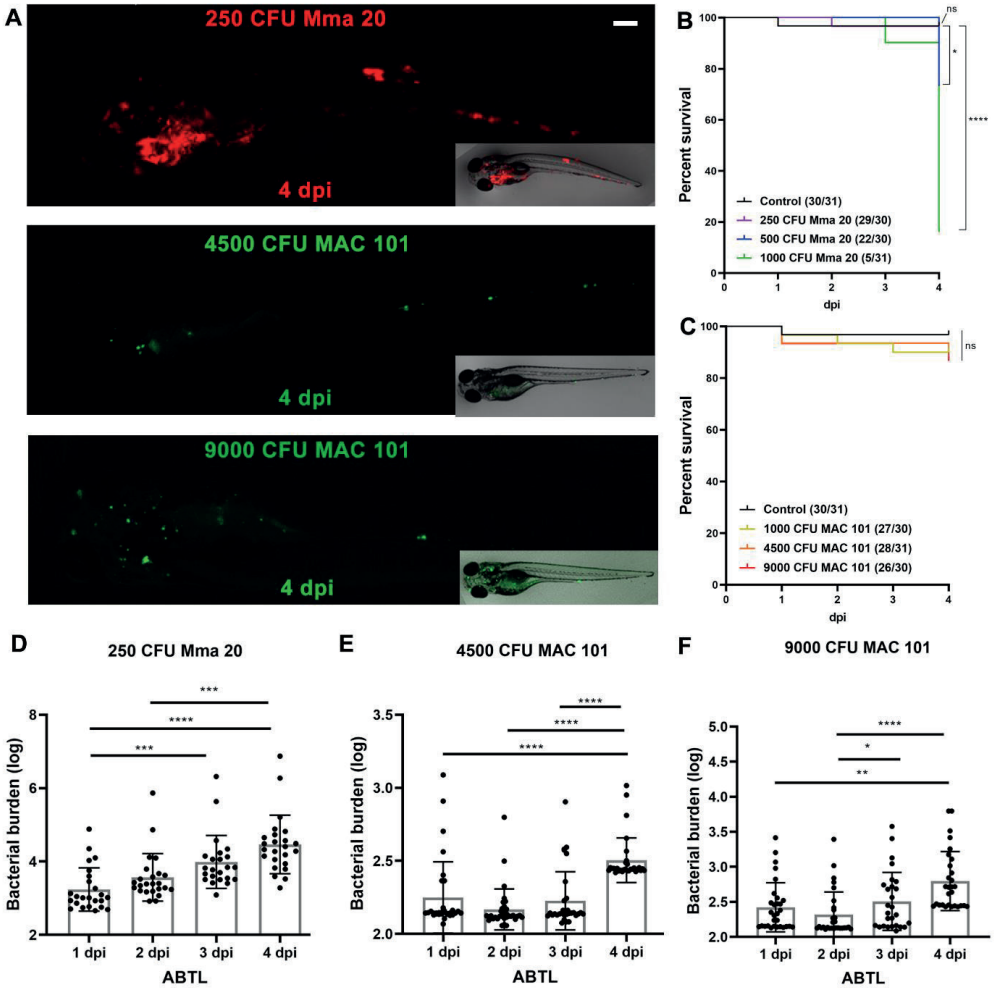

Figure 1 Quantification of bacterial burden and survival after *M. marinum* or *M. avium* infection. ABTL zebrafish larva infected with mCherry-labeled *M. marinum* Mma 20 at a dose of ~250 CFU and infected with wasabi-labeled *M. avium* MAC 101 at a dose of ~ 4500 CFU or 9000 CFU by caudal vein infection at 28 hpf. (A) Representative images for the bacterial burden quantification were taken at 4 dpi. (B, C) Percent of survival curves for ABTL zebrafish larva infected with a series of does *M. marinum* Mma20 or *M. avium* MAC 101. (D) Bacterial burden quantification of ABTL zebrafish larvae upon ~250 CFU Mma 20 infection. (E) Bacterial burden quantification of ABTL zebrafish larvae upon ~4500 CFU MAC 101 infection. (F) Bacterial burden quantification of ABTL zebrafish larvae upon ~9000 CFU MAC 101 infection. In (B, C) data were collected from three pools of zebrafish larvae. In (D, E, and F) data (mean ± SD) were combined from three pools of zebrafish larvae. Statistical significance of differences was determined by unpaired t-test for comparison between the *tlr2* mutant and its wild type sibling group. *, $P < 0.05$, **, $P < 0.01$, ***, $P < 0.001$, ****, $P < 0.0001$. Scale bar: 50 µm. Sample size (n): 24, 24, 23, 24 (C), 31, 33, 31, 30 (D), 30, 29, 27, 29 (E). Scale bar: 50 µm.

M. avium is persisting in macrophages that form granuloma-like clusters

Although granulomas are regarded as host-defensive structures historically, they can prevent drugs from penetrating the bacteria inside of them and make therapeutic treatment of NTM infection challenging [4]. It has been demonstrated that macrophages play a dominant role in initiating the granuloma formation at the early *M. marinum* infection stage in zebrafish embryos [19, 31]. However, the information about granuloma formation upon *M. avium* infection is limited. In order to investigate the role of macrophages in MAC 101 granuloma formation we used larvae of the *Tg(Mpeg1:EGFP)* zebrafish line, in which macrophages express EGFP. We infected the larvae in the same manner as before, with ~250 CFU *M. marinum* Mma20 or ~4500 CFU *M. avium* MAC 101 respectively, and observed the appearance of granuloma-like clusters (Fig. 2). While both infections exhibited clear overlap between bacteria and clusters of macrophages at 4 dpi, the Mma20 infection showed more extracellular bacteria and cording morphology (Fig. 2A), while larvae infected with MAC 101 exhibited more intracellular bacteria (Fig. 2B). This result suggests that the granuloma structures caused by *M. avium* infection are more sealed compared to the granulomas resulting from *M. marinum* infection.

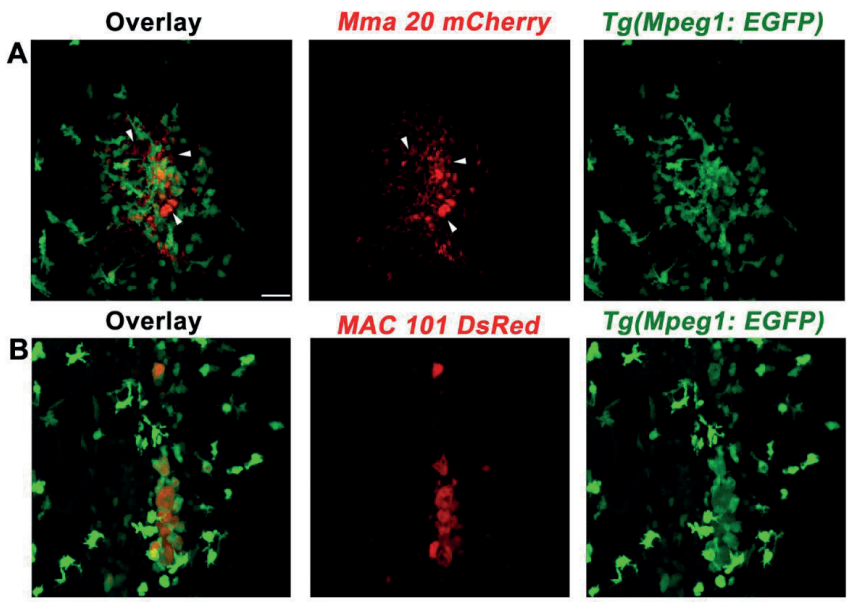

Figure 2 The comparison of granuloma-like cluster phenotypes in wild type transgenic line *Tg(Mpeg1: EGFP)* zebrafish larvae upon *M. marinum* Mma20 or *M. avium* MAC 101 infection. (A) A representative CLSM image of *Tg(Mpeg1: EGFP)* zebrafish larva infected with mCherry-labeled Mma20 strain. *Tg(Mpeg1: EGFP)* embryos were infected ~250 CFU Mma20 mCherry strain at 28 hpf. CLSM imaging was performed with the infected larvae at 4 dpi with 40 times magnification lens (oil immersion, N.A. 1.3). (B) A representative CLSM image of *Tg(Mpeg1: EGFP)* zebrafish larva infected with DsRed-labeled MAC 101 strain. ~4500 CFU MAC 101 DsRed strain was injected in 28 hpf *Tg(Mpeg1: EGFP)* zebrafish embryos. CLSM images were taken for the 4 dpi MAC 101 infected larvae by using 20 times magnification lens (oil immersion, N.A. 1.3). The white arrow represents the bacteria outside macrophages. Scale bar: 50 µm.

Transcriptional difference between *M. marinum* and *M. avium* infected zebrafish larvae

To gain a better understanding of the differences in host responses to Mma20 versus MAC 101 we performed transcriptome analysis of zebrafish larvae infected with MAC 101 by RNAseq. MAC 101 infected and PBS-injected control groups were collected for RNA isolation at 4 dpi and used to create RNAseq libraries. We compared the results to published RNAseq datasets of 4 dpi larvae infected with ~250 CFU *M. marinum* Mma20 versus PBS, from NCBI (GEO database accession for the RNASeq data: GSE76499) [32]. When comparing the previously published RNAseq data of 4 dpi Mma20 infection larvae to that of PBS-injected control group [32] , we found 1164 genes upregulated and 772 genes downregulated (Fig. 3A). A different response was observed when larvae were challenged with ~4500 CFU *M. avium* MAC 101, which exhibited 5244 upregulated genes and 4978 downregulated genes (Fig. 3A). To investigate the overlap of genes regulated by the two mycobacteria, we plotted three Venn diagrams. The results show that 1270 genes (12.4% in MAC 101 *vs* PBS group, 65.6% in Mma20 *vs* PBS group) are regulated by both Mma20 and MAC 101, 696 upregulated genes were shared, while only 410 common downregulated genes were found. For further analysis, we classified the differential regulated genes according to the KEGG pathway by using the online functional classification tool Database for Annotation, Visualization and Integrated Discovery (DAVID; http://david.abcc.ncifcrf.gov/summary.jsp). The analysis showed that most DEGs were enriched in metabolism-related pathways in MAC 101 vs PBS group (Fig. S1B). Moreover, we further compared the enriched pathways by using the Venn diagram. We found that there were 6 enriched pathways the same: ECM-receptor interaction; Focal adhesion; Glycine, serine and threonine metabolism; Glutathione metabolism; Arginine and proline metabolism and Tryptophan metabolism. These results indicate that zebrafish larvae have a different transcriptome response to MAC 101 infection.

Common and specific gene expression profiles in toll-like receptor signaling pathway after *M. marinum* and *M. avium* infection

Innate immune responses are important to protect the host from NTM infection, which is mainly mediated by the toll-like receptor (TLR) signaling pathway [33-35]. We wanted to compare the transcriptomic profiles of the host responses to the infections specifically in relation to TLR signaling. Thus, we visualized the DEGs that are characterized as being part of or downstream of TLR signaling pathways (Fig. S2 and Fig. 4) for the two mycobacterial infections.

In Fig. 4, the categories of Cytokines and chemokines; Cytokine and chemokine receptor; Autophagy regulators; Transcription factors; Blood factors; Complement cascade; Matrix remodeling and Mitochondrial were analyzed and visualized by the program Pathvisio. In each category, we summarized common regulated gene set, specific regulated gene set in Mma20 infection group, specific regulated gene set in MAC 101 infection group, and different regulated gene set. In the category of the Cytokines and chemokines, we found *tnfb*, *il1b*, *lepb*, *il12a*, *cxcl8b*, *cxcl8b.1*, *cxcl8a*, *ccl19a.1*, and *csf3b* were upregulated to respond to both Mma20 and MAC 101 infection. *Tnfa*, *cxcl19*, *cxcl19b*, *cxck20*, *ccl34b.8*, and *ccl34a.4* were specifically upregulated in Mma20 infection group. *Cxcl14*, *cxcl8b.3*, and *ccl25b* were specifically regulated, while *cxcl11.7*, *ccl36.1*, *cxcl12b*, *ccl33.3* were specifically downregulated in MAC 101 infection group. Interestingly, *ccl34b.1* was downregulated in Mma20 infection group but was upregulated in MAC 101 infection group. In the categories of Cytokine and chemokine receptors, Autophagy regulators and Matrix remodeling, we found that there were more genes only significantly responded to the MAC 101 infection. In the Blood factors category, *hp* was upregulated in Mma20 infection group. In contrast, *hp* was downregulated in MAC 101 infection group (Fig. 4).

Overall, the transcriptomic profile of genes characterized as functioning downstream of TLR signaling pathways showed divergences in all functional classes of genes, but particularly in cytokines and chemokines, autophagy regulators, and genes involved in matrix remodeling. This further underscores that the host immune response is different between Mma20 and MAC 101.

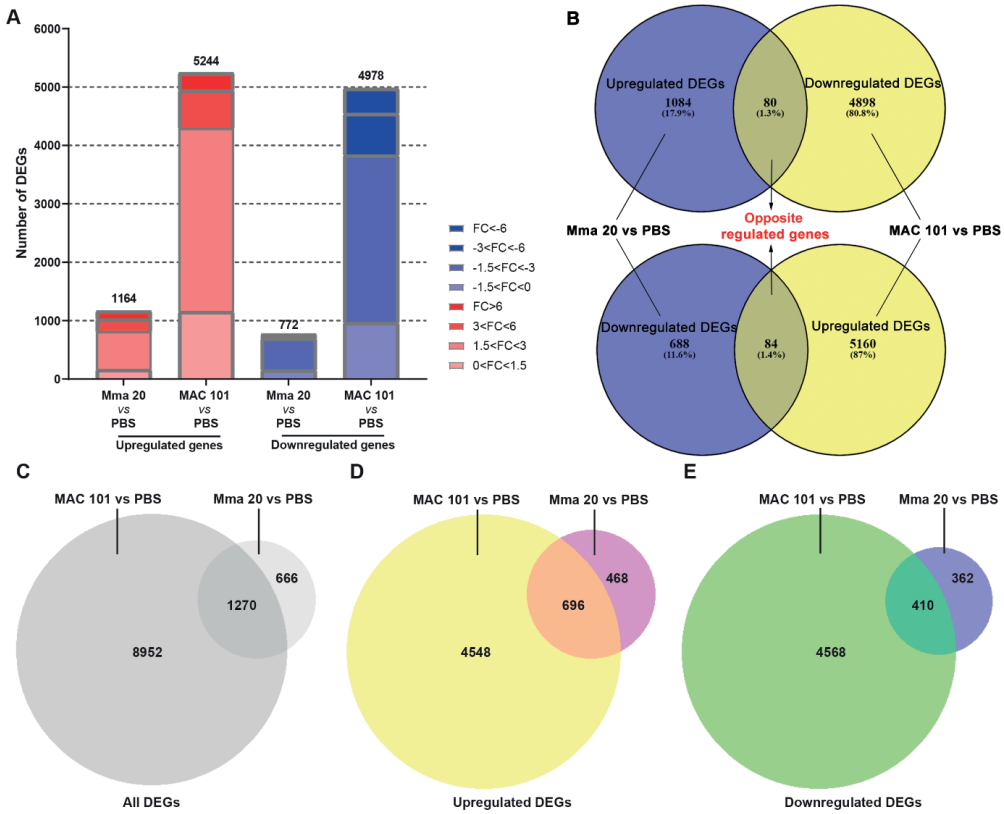

Figure 3 The global comparative analysis of the differential expressed genes (DEGs) in zebrafish larvae upon *M. marinum* Mma20 or *M. avium* MAC 101 infection. AB/TL zebrafish embryos were injected with ~250 CFU *M. marinum* Mma20 strain (GEO database accession for RNA-Seq: GSE76499 [32]) or ~4500 CFU *M. avium* MAC 101 strain at 28 hpf, respectively. The embryos in the control group were injected with PBS. The samples for RNAseq are taken from three independent sample sets with the infected larvae at 4 dpi. (A) Overview of the distribution of DEGs fold change in zebrafish larvae infected with Mma 20 or MAC 101. DEGs were assessed by FDR p-value < 0.05. Upregulated gene sets are shown in red and downregulated gene sets are shown in blue. The intensity of the color represents the fold change level. (B) Venn diagram shows the opposite regulated DEGs. (C- E) Venn diagram shows the common and specific gene numbers of all DEGs (C), upregulated DEGs (D), and downregulated DEGs (E) between Mma20 vs PBS and MAC 101 vs PBS groups. The Venn diagrams were made by the website: https://www.biovenn.nl/.

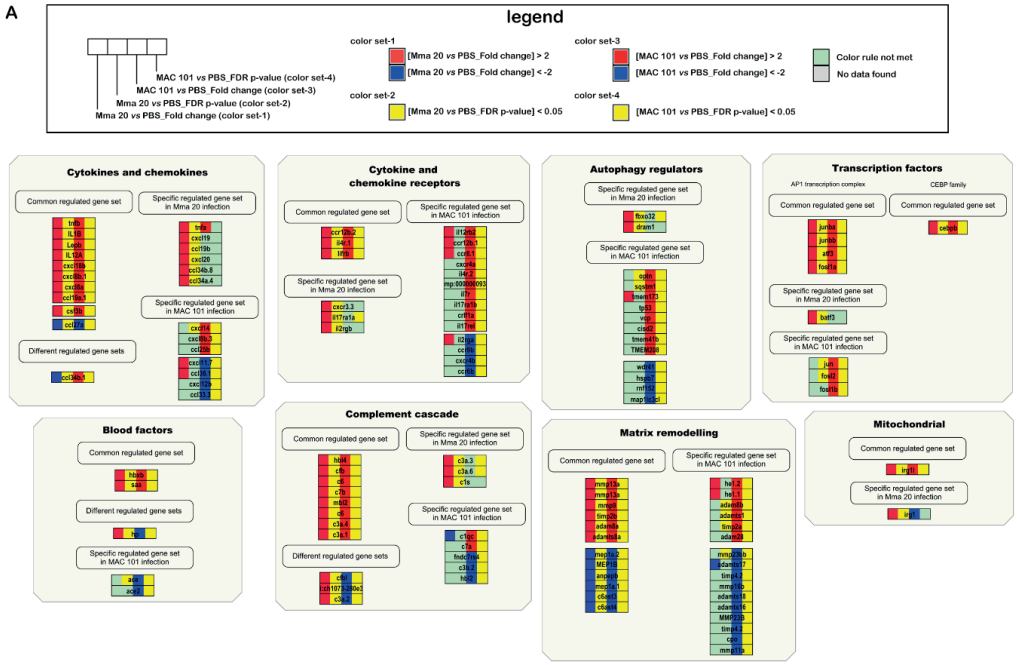

Figure 4 Inflammatory response genes in the transcriptome of larvae infected with *M. marinum* Mma20 or *M. avium* MAC 101. The pathway was adapted from the Wiki pathway. In the visualization, the gene expression in the comparison of Mma20 infection *vs* PBS and MAC 101 infection *vs* PBS are depicted by color (red, upregulated; blue, downregulated; yellow, FDR *p*-value < 0.05).

M. marinum and *M. avium* infection in *tlr2* mutant larvae

Having established that the TLR associated transcriptomic profiles of the host responses to the two mycobacterial infections differ, we wanted to address this in more detail. Previous studies by our group have demonstrated that *tlr2* is important for the ability of zebrafish larvae to control *M. marinum* infection, a phenomenon which can be explained by the effect on metabolic pathways and the presence of higher extracellular bacterial burden in the *tlr2* mutants [36]. To further explore the role of *tlr2* in the control mycobacterial infection, we investigated whether *tlr2* is also involved in the immune response to *M. avium* infection.

To compare the role of *tlr2* in *M. marinum* and *M. avium* infection, we injected ~250 CFU Mma20 or ~4500 CFU MAC 101 into *tlr2* loss-of-function mutants and their wild type siblings. Images of infected larvae were taken at 1 dpi and 4 dpi to assess the bacterial burden by integrated intensity. In both cases, the bacterial burden was significantly increased at 4 dpi in the *tlr2* deficient background (Fig. 5). This increased bacterial burden in the *tlr2* mutant could be caused by inability of macrophages to clear bacteria. To confirm this, we analyzed

macrophage behavior upon infection by confocal microscopy, using *tlr2*$^{+/+}$ *Tg (mpeg1:EGFP)* and *tlr2*$^{-/-}$ *Tg (mpeg1:EGFP)* infected *M. avium* MAC 101 strain (Fig. 6). Surprisingly, the bacterial pixel count within macrophages was significantly higher in the *tlr2* mutant. There was no statistically significant difference between *tlr2* mutants and WT siblings in the bacterial burden outside of macrophages. In previous work, we found that Mma20 bacterial fluorescent signal was significantly elevated outside of macrophages in *tlr2* mutants compared with its heterozygote and wild type sibling controls [36], but no significant difference was found in the intracellular bacterial pixel count (data are not shown). This finding indicates a *tlr2* related difference in the host response to MAC 101 compared to Mma20.

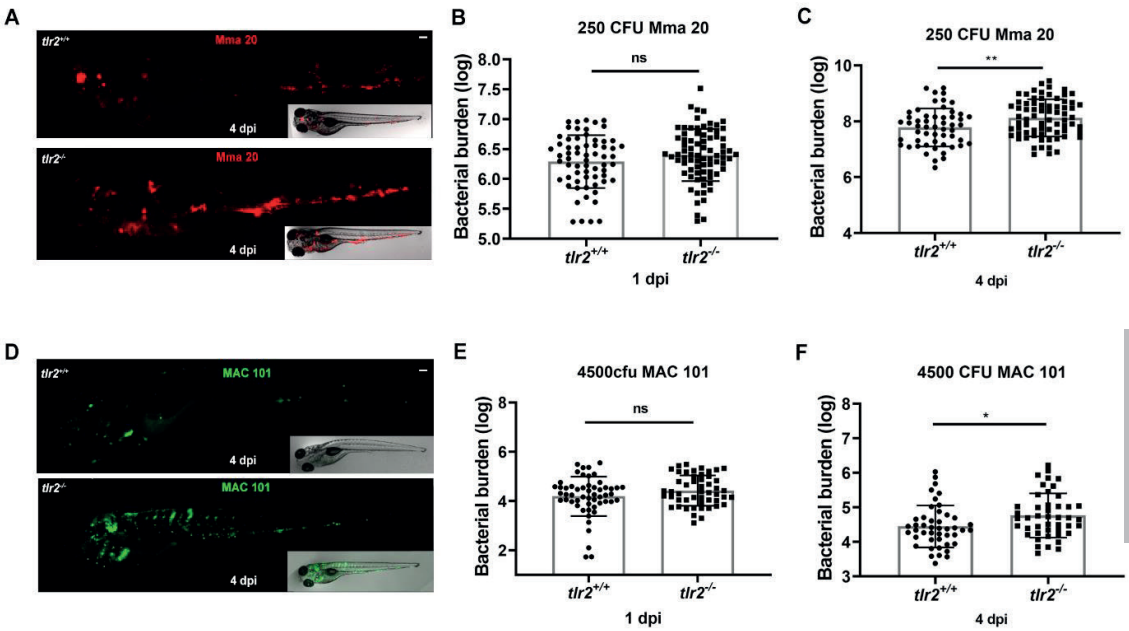

Figure 5 Quantification of bacterial burden in *tlr2* zebrafish larvae with *M. marinum* Mma20 or *M. avium* MAC 101 infection. *Tlr2*$^{+/+}$ and *tlr2*$^{-/-}$ embryos were infected at 28 hpf by caudal vein infection with mCherry-labeled *M. marinum* strain Mma20 at a dose of ~ 250 CFU, or infected with ~ 4500 CFU wasabi-labeled *M. avium* strain MAC 101. (A) Representative images of *tlr2*$^{+/+}$ and *tlr2*$^{-/-}$ embryos infected with mCherry-labeled *M. marinum* strain Mma20 at 4 dpi. (B) Quantification of bacterial burden of *tlr2*$^{+/+}$ and *tlr2*$^{-/-}$ upon Mma20 infection at 1 dpi. (C) Quantification of bacterial burden of *tlr2*$^{+/+}$ and *tlr2*$^{-/-}$ upon Mma20 infection at 4 dpi. (D) Representative images of *tlr2*$^{+/+}$ and *tlr2*$^{-/-}$ embryos infected with wasabi-labeled *M. avium* strain MAC 101 at 4 dpi. (E) The bacterial burden of *tlr2*$^{+/+}$ and *tlr2*$^{-/-}$ upon MAC 101 infection were quantified at 1 dpi. (F) The bacterial burden of *tlr2*$^{+/+}$ and *tlr2*$^{-/-}$ upon MAC 101 infection were quantified at 4 dpi. In (B, C, and E, F) data (mean ± SD) were combined from three independent experiments. Statistical significance of differences was determined by unpaired t-test for comparison between the *tlr2* mutant and its wild type sibling group. ns, non-significant; *, $P < 0.05$, **, $P < 0.01$. Scale bar: 50 µm. Sample size (n): 64, 78 (B), 54, 72 (C), 54 , 50 (E), and 45, 45 (F)

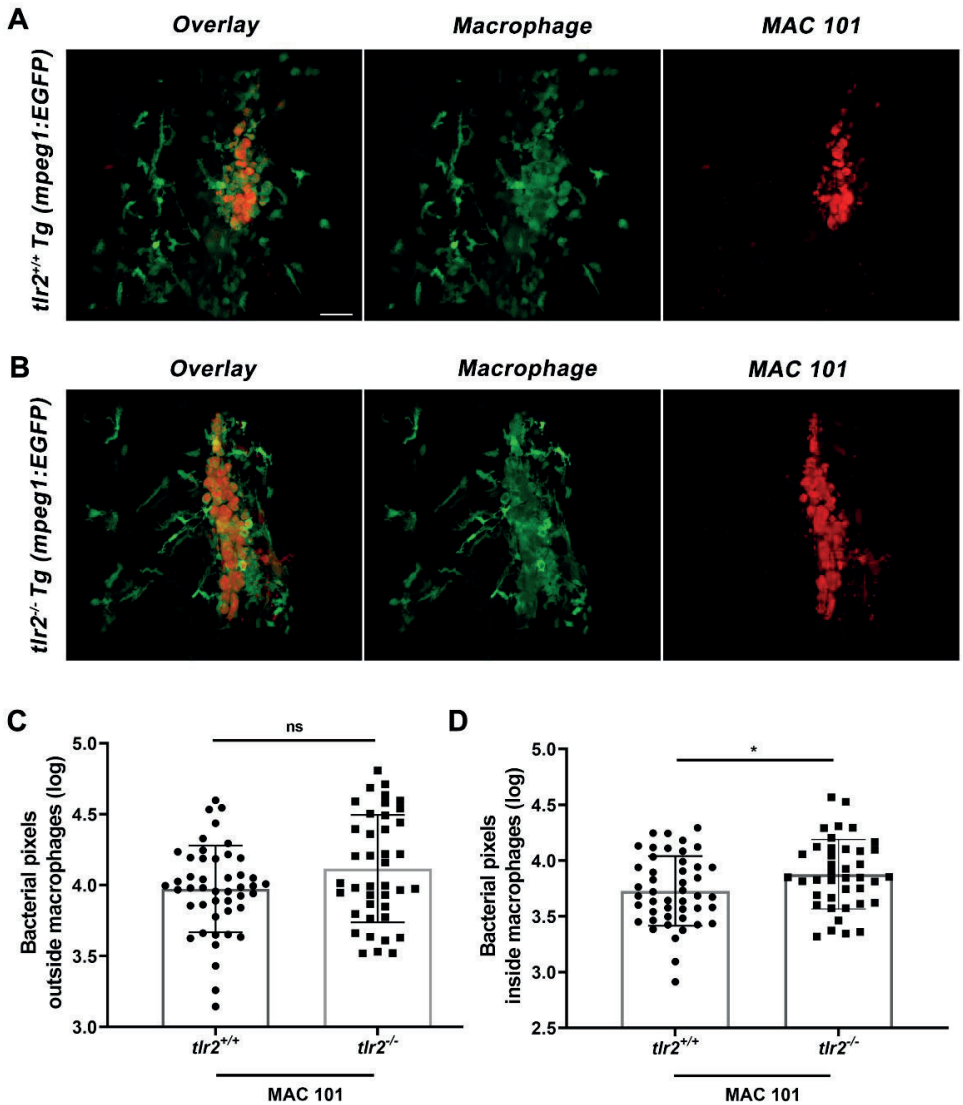

Figure 6 Quantification of the extracellular and intracellular bacterial burden in the *tlr2* mutant upon *M. avium* infection. *Tlr2*$^{+/+}$ *Tg(Mpeg1: EGFP)* and *tlr2*$^{-/-}$ *Tg(Mpeg1: EGFP)* zebrafish embryos were infected with ~4500 CFU MAC 101 DsRed strain at 28 hpf by caudal vein infection. (A, B) Representative CLSM images of *tlr2*$^{+/+}$ *Tg(Mpeg1: EGFP)* and *tlr2*$^{-/-}$ *Tg(Mpeg1: EGFP)* zebrafish larvae infected with DsRed-labeled *M. avium* MAC 101 strain. CLSM imaging was performed with the infected larvae at 4 dpi with 40 times magnification lens (oil immersion, N.A. 1.3). (C) Quantification of bacteria outside macrophages by pixel count. (D) Quantification of bacteria inside macrophages by pixel count. In (C and D) data (mean ± SD) were combined from two independent experiments. Statistical significance of differences was determined by unpaired t-test for comparison between the *tlr2* mutant and its wild type sibling group. ns, non-significant; *, $P < 0.05$. Sample size (n): 46, 40 (C, D). Scale bar: 30 µm.

Different migratory behavior of macrophages and neutrophils after *M. marinum* and *M. avium* infection in *tlr2* mutant larvae

Some studies have demonstrated that the migration of leukocytes during the infection process is important for bacterial clearance, containment, dissemination, and granuloma formation at the early mycobacterial infectious stage [37-40]. We have previously shown that *tlr2* is involved in regulating leukocyte migration in response to inflammatory signaling [29]. We hypothesized that *tlr2* could also be involved in the regulation of migratory behavior of macrophages and neutrophils to the sites of mycobacterial infection.

To test the hypothesis, we applied the tail fin infection model which was described before [37, 41]. This model has unique advantages in studying cell tracking. The tail fin of zebrafish larvae is a very thin tissue which contains mesenchymal cells, extracellular collagenous fibers, and an epidermis [42]. The thin tail fin makes it possible to set short time interval when the cell tracking was performed by CLSM, enabling high accuracy of tracing individual cells. Representative images of this tail fin infection model are shown in Fig. 7. mCherry labeled Mma20 or DsRed labeled MAC 101 were locally injected into the tail fin by using the 2 dpf zebrafish larvae. The region of the tail fin was imaged by using CLSM at 3 dpi.

To assess the role of *tlr2* mutation in regulating the recruitment of macrophages and neutrophils to the sites of the infection, Alexa Fluor dye stained Mma20 or MAC 101 were injected into 3 dpf *tlr2*$^{+/+}$ *Tg (mpeg1:mCherry-F);TgBAC (mpx: EGFP)* and *tlr2*$^{-/-}$ *Tg (mpeg1:mCherry-F);TgBAC (mpx: EGFP)* larvae. Time-lapse microscopy was performed by using CLSM between 1 hpi to 3 hpi. The time-lapse images were analyzed by Imaris to quantify the number, the speed of migration and meandering index of recruited leukocytes to the granuloma-like structures in the tail fin region (Fig. 8 and 9). We found that the recruited macrophages were fewer in numbers in the *tlr2* mutants upon Mma20 and MAC 101 infection compared with wild type sibling controls (Fig. 8 A-C). Interestingly, fewer macrophages were recruited to the MAC 101 site of infection in wild type sibling larvae compared to Mma20 wild type larvae (Fig. 8 A-C). We further quantified the speed and meandering index of the macrophages in the tail region. In the Mma20 infection group, macrophages in *tlr2*$^{-/-}$ group move significantly slower than the macrophages in it wild type sibling group, whereas no difference of meandering index was found (Fig. 8 D, E). In contrast, no significant difference was found in the speed of *tlr2*$^{+/+}$ macrophages and *tlr2*$^{-/-}$ macrophages after MAC 101 infection, while the meandering index of *tlr2*$^{-/-}$ macrophages is decreased after MAC 101 infection (Fig. 8 D, E). Interestingly, the mean

speed and meandering index of macrophages in Mma20 infection groups are always higher than the macrophages in their corresponding genotype MAC 101 infection groups (Fig. 8 D, E).

Comparing the behavior of neutrophils, we found that fewer neutrophils were recruited to the infected tail fin in Mma20 infected *tlr2*$^{+/+}$ group compared to the *tlr2*$^{-/-}$ at early time points (Fig. 9 A, C). In contrast, higher numbers of neutrophils were recruited in *tlr2*$^{+/+}$ compared to the *tlr2*$^{-/-}$ MAC101 infection group although the difference in the number of neutrophils becomes smaller in the later stage of the tracking among the four groups. We found that the mean speed and meandering index in the *tlr2*$^{-/-}$ neutrophils are decreased after Mma20 infection (Fig. 9 D, E). However, no difference in mean speed and the meandering index was observed between the *tlr2* mutant and its wild type siblings after MAC 101 infection (Fig. 9 D, E). The same to what we found in macrophages, the mean speed and meandering index of neutrophils in the Mma20 infection groups are always higher than of the neutrophils in the MAC 101 infection groups.

We found no difference in recruited leukocyte numbers, mean speed and meandering index of macrophages and neutrophils between *tlr2*$^{+/+}$ and *tlr2*$^{-/-}$ after PBS mock injection, which demonstrates that the differences observed above are depended on *tlr2* mutation and different mycobacteria, and not the damage of the injection (Fig. S3). To confirm the results we got from Imaris analysis, we used the Track Foci plug-in [43] (Fig. S4). The result of Track Foci, we found the overall mean speed of both macrophages and neutrophils is faster in the *tlr2*$^{+/+}$ Mma20 infection group compared to the *tlr2*$^{-/-}$ Mma20 infection group and *tlr2*$^{+/+}$ MAC 101 infection group respectively, which is consistent with what we observed by the Imaris analysis (Fig. S4). In conclusion, the results suggest that *tlr2* regulates the macrophages and neutrophils in different ways after different mycobacterial infections.

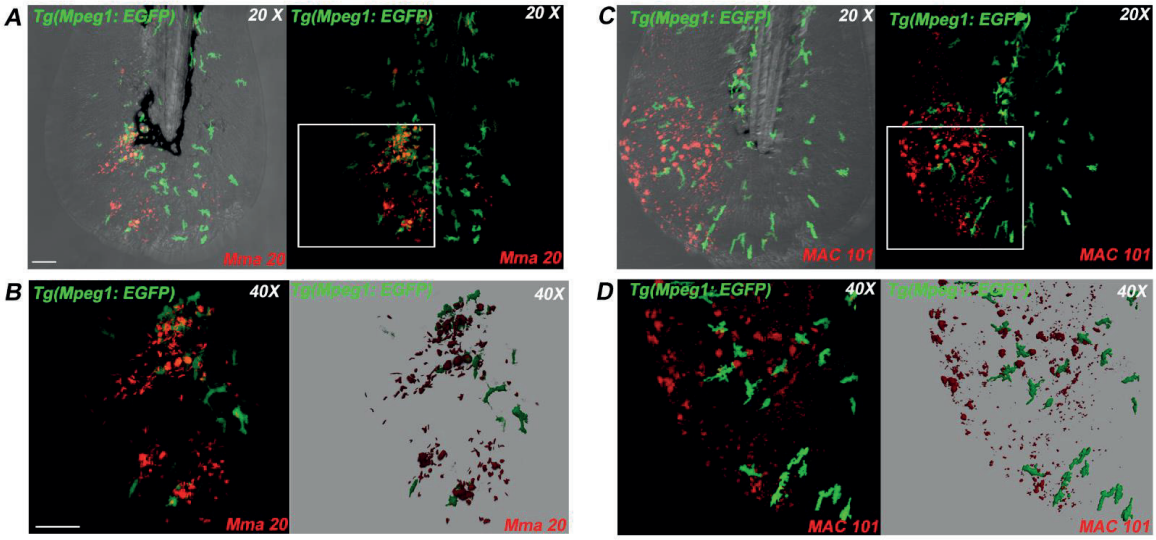

Figure 7 The tail fin infection model. (A, B) Representative images of *Tg (Mpeg1:EGFP)* larva infected with mCherry-labeled *M. marinum* strain Mma20 by tail fin injection. In A, The 3 dpi *Tg (Mpeg1:EGFP)* larva with tail fin Mma20 infection was imaged by using CLSM (20X, N.A. 0.75). The higher magnification image (40X, oil immersion, N.A. 1.3) in the white box area of (A) is shown in (B). (C, D) DsRed-labeled *M. avium* strain MAC 101 tail fin infected *Tg (Mpeg1:EGFP)* larva was imaged at 3 dpi in the tail fin region by using CLSM (20X, N.A. 0.75). A higher magnification image (40X, oil immersion, N.A. 1.3) in the white box area of (C) is shown in (D). In (A, C), the right panel is the image without a bright field. In (B, D), the right panel images are the 3D version of the left panel built by Imaris x64 7.4. Scale bar: 50 µm.

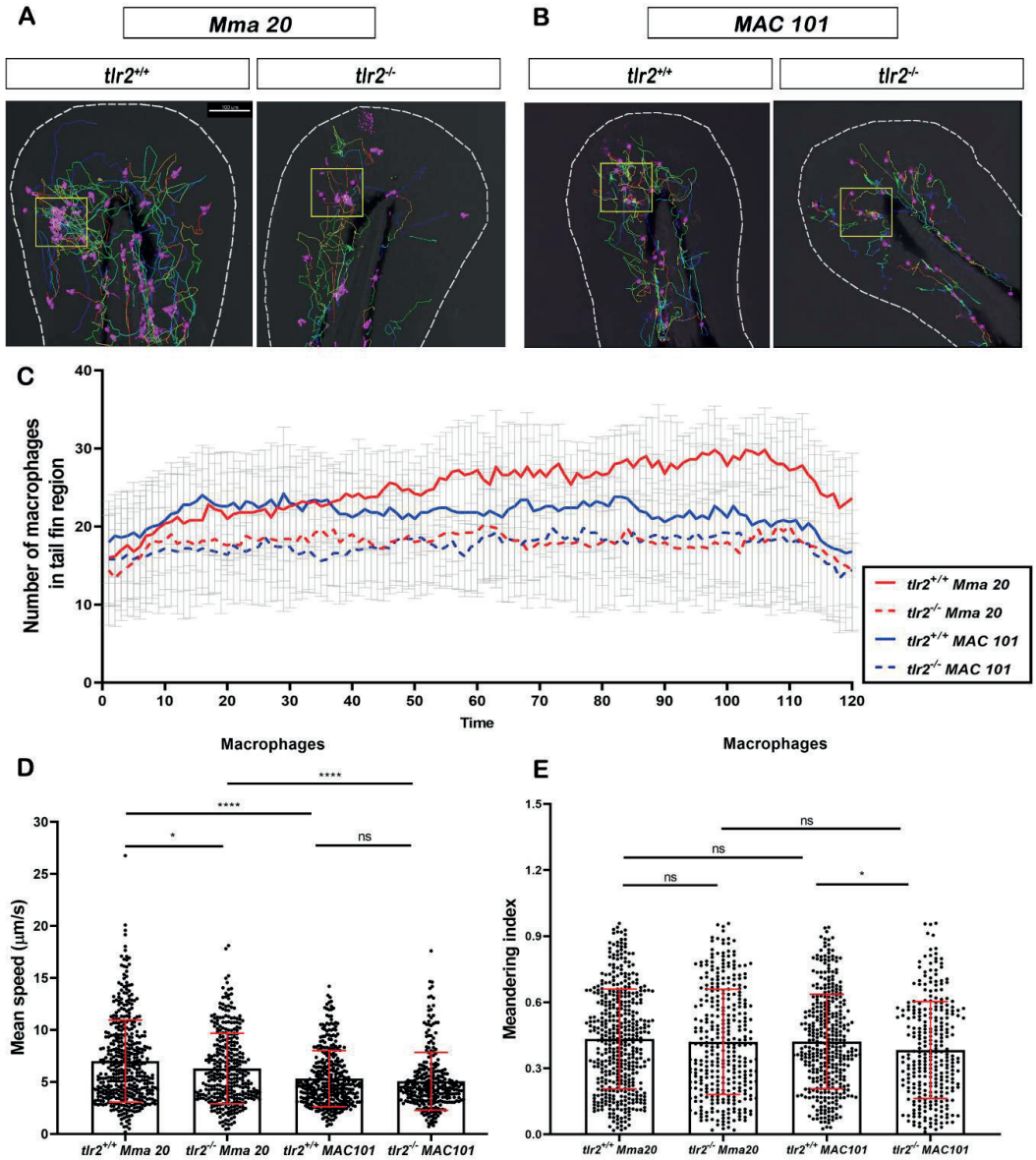

Figure 8 Quantification of macrophages behavior in *tlr2* mutant and sibling control larvae after *M. marinum* Mma20 or *M. avium* MAC 101 tail fin infection. (A) Representative images of macrophage tracks in $tlr2^{+/+}$ or $tlr2^{-/-}$ larvae with Mma20 tail fin infected. (B) Representative images of macrophage tracks in $tlr2^{+/+}$ or $tlr2^{-/-}$ larvae with MAC 101 tail fin infected. In (A, B), the magenta balls represent the tracked macrophages, the yellow box indicates the infected area. (C) The number of recruited macrophages to the tail fin region upon Mma20 or MAC 101 infection. The curves represent the mean value of the recruited neutrophil numbers at different time points. (D) The mean speed of tracked macrophages in infected tail fin region. (E) The meandering index of tracked macrophages in infected tail fin region. In (D, E) data (mean ± SD) were combined from three independent experiments with 5 fish in each group. An unpaired, two-tailed t-test was used to assess significance. ns, non-significant; *, $P < 0.05$, ****, $P < 0.0001$. Scale bar: 100 μm; Sample size (n): 447, 343, 372, 290 (D, E).

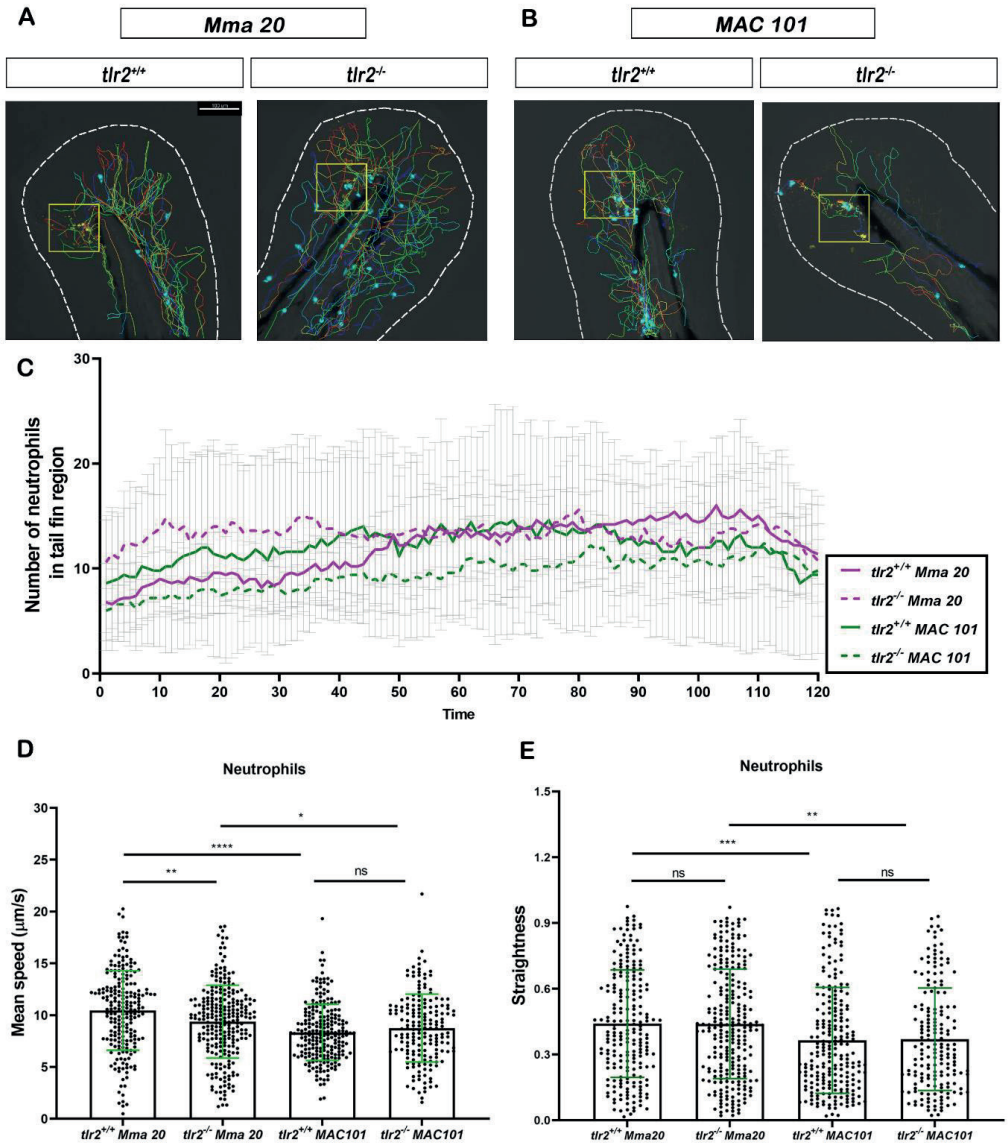

Figure 9 Quantification of neutrophils behavior in *tlr2* mutant and sibling control larvae after *M. marinum* Mma20 or *M. avium* MAC 101 tail fin infection. (A) Representative images of neutrophil tracks in *tlr2*$^{+/+}$ or *tlr2*$^{-/-}$ larvae with Mma20 tail fin infected. (B) Representative images of neutrophil tracks in *tlr2*$^{+/+}$ or *tlr2*$^{-/-}$ larvae with MAC 101 tail fin infected. In (A, B), the cyan balls represent the tracked neutrophils, the yellow box indicates the infected area. (C) The number of recruited neutrophils to the tail fin region upon Mma20 or MAC 101 infection. The curves represent the mean value of the recruited neutrophil numbers at different time points. (D) The mean speed of tracked neutrophils in infected tail fin region. (E) The meandering index of tracked neutrophils in infected tail fin region. In (D, E) data (mean ± SD) were combined from three independent experiments with 5 fish in each group. An unpaired, two-tailed t-test was used to assess significance. ns, non-significant; *, $P < 0.05$, ****, $P < 0.0001$. Scale bar: 100 μm; Sample size (n): 217, 254, 228, 179 (D, E)

Discussion

The investigation of the infectious diseases caused by nontuberculous mycobacteria (NTM) is receiving increasing attention because the disease prevalence has been increasing sharply since 2000 [44]. The bacteria belonging to the *M. avium* complex (MAC) are the most important pathogens for NTM infectious disease, accounting for 80% of NTM infectious disease cases [45, 46]. However, our understanding of the MAC infection mechanism is incomplete. *M. marinum*, that is genetically close related to the *M. tuberculosis* complex is widely utilized to model human tuberculosis *in vivo* [47]. Many new insights have been obtained in the last decades in our understanding of tuberculosis disease progression by using *M. marinum* infection in a zebrafish model [21, 22]. It could help us further uncover the pathobiology of MAC infectious diseases by comparing *M. avium* infection with *M. marinum* infection. In this study, we applied the zebrafish infection model to study the formation of granuloma-like cluster by CLSM imaging and investigate the host response to the infection through RNAseq analysis. In the first place we compared the difference between the *M. marinum* Mma20 and *M. avium* MAC 101 infection processes. Secondly, we focused on the function of toll-like receptor signaling after Mma20 and MAC 101 infection to compare the function of Tlr2 in infection with two different bacteria.

M. marinum Mma20 is more virulent than *M. avium* MAC 101

NTM are intracellular pathogens and macrophages are the first responders to defend against NTM at the early infection stage [48]. In this study, we found that MAC 101 is persisting in the macrophages with less extracellular cording compared to Mma20 (Fig. 2). Extracellular cording is a morphology of mycobacteria accompanied by necrotic macrophages and extracellularly replicating bacteria which prevent phagocytosis because of the size of the clusters [49, 50]. Bacterial cording is a pathogenic feature associated with hyper-virulence in *M. tuberculosis*, *M. marinum*, *M. abscessus*, *M. fortuitum*, and *M. chelonae* [49, 51-54]. Thus, Mma20 infected larvae presenting more extracellular cords may be a feature of the higher lethality and bacterial growth in Mma20 infection (Fig. 1 and 2). It is widely believed that macrophages play a protective role during mycobacterium infection. Macrophages execute a series of functions including recognizing mycobacteria, forming granulomas, and eliminating bacteria [48]. However, mycobacteria have evolved the ability to evade the immune system by using macrophages as a safe haven [55, 56]. This safe haven in the form of a granuloma affects drug delivery into the mycobacteria inside it and then makes them drug-tolerant [4]. Moreover,

granulomas can also provide a favorable environment for mycobacteria to survive longer inside the host [57]. Thus, more closed granuloma-like clusters in MAC 101 infection might contribute to a slower disease progression in MAC infectious diseases and the difficulties in treatment. The MAC 101 zebrafish infection model is therefore suitable to be further applied to study the host-mediated mechanism of drug tolerance in macrophages.

Different transcriptome responses to infection by *M. avium* MAC 101 and *M. marinum* Mma20

In general, we found that *M. avium* MAC 101 infection induced more innate immune responses, including a higher number of significantly regulated genes from the categories of cytokines, chemokines, and their receptors, autophagy regulators, blood factors, complement cascade and matrix remodeling. It should, however, be noted that as the transcriptomic dataset of the Mma20 response has been reanalyzed from a previous publication [32], and therefore a number of technical factors may have contributed to the apparent difference in the magnitude of the host transcriptomic response. In the category of cytokines, chemokines and their receptors, we found more genes were downregulated specifically in the MAC 101infection group, e.g. *il1rga*, *ccr9b*, *cxcr4b*, *ccr6b*, *cxcl11.7*, *ccl36.1*, *cxcl12.b* and *ccl33.3* (Fig. 4). Interestingly, we found that Cxcr4b/Cxcl12 signaling was downregulated in the MAC 101 infection group. CXCR4 signaling is well known to relate to HIV pathogenesis, tumor-sustained angiogenesis and mycobacteria-induced angiogenesis [58-60]. Deficiency of *cxcr4b* has been shown to delay *M. marinum* growth in zebrafish larvae through effects on granuloma-associated angiogenesis [60]. Additionally, Doncker et al. reported that AIDS patients with disseminated MAC infection are associated with CXCR4 dysfunction, which seriously affected the internalization promoted by CXCL12, but with normal membrane CXCR4 expression on the leukocytes surface [61]. In contrast, *cxcr4a* was upregulated in zebrafish larvae upon MAC 101 infection, which indicates that *cxcr4a* and *cxcr4b* may have antagonistic functions to mycobacterial infection (Fig. 4). These studies suggest that CXCR4 signaling play a role during MAC 101 infection. However, the function of CXCR4 upon MAC infection is still not clear and merits further studies. Furthermore, it has been demonstrated that CXCR4/CXCL12 signaling sustains leukocytes trafficking to inflammatory sites as well as CXCL11 signaling which mediates the recruitment of macrophages upon mycobacterial infection [62, 63]. Thus, we hypothesize that the macrophage and neutrophil migration behavior can be different in zebrafish larvae after infection with different NTM. The cell tracking experiments in this report (Fig. 8 and Fig. 9)

confirmed this hypothesis. Lower numbers of recruited macrophages were observed in MAC 101 infection regions compared to Mma20 infection regions, while the number of recruited neutrophils was not different. The migration speed of neutrophils to infection regions was decreased (Fig. 7 and 8). This will be discussed further below.

The complement system is a critical part of the innate immune system and plays a role in mediating the leukocyte function upon mycobacterial infection. For example, mycobacteria can utilize complement receptors, like the complement receptor types 1, 3 and 4 (CR1, CR3 ,CR4) to enter the macrophages [64]. In this study, we found several complement components regulated in different ways in response to different mycobacterial infections, e.g. *c3b.2* which specifically responded to MAC 101 (Fig. 4). It has been demonstrated by Schorey et al. that pathogenic mycobacteria including *M. tuberculosis*, *M. leprae*, and *M. avium* share the same macrophage invasion mechanism [65, 66]. The generation of C3b is induced upon mycobacterial infection to promote the uptake of the invading mycobacteria by macrophages [65]. These results also indicated that C3b was the predominant *M. avium* opsonin, which provides a link with our results [65]. However, the research of the link between the complement system and *M. avium* infection still has some contradictory points. Bohlson et al. found that the induction of TNF-α in C3 deficient mice was of a similar level as in C3 wild type mice and there was no difference in bacterial burden, which indicates that the major effector function of complement is not necessary to control *M. avium* infection [13]. On the contrary, Irani et al. reported that the synthesis of TNF-α in *M. avium*-infected mice macrophages is C3-dependent [14]. Considering that it is likely that the main reason for the difference between these reports is that they used different subtypes of *M. avium*, the link between MAC infection and the complement system, needs to be further confirmed.

Tlr2 plays a role in defense against different mycobacterial species

In the present study, we found that *tlr2*$^{-/-}$ zebrafish larvae showed a higher bacterial burden compared to their wild type sibling controls after either *M. marinum* Mma20 or *M. avium* MAC 101 infection. The results with Mma20 are consistent with what we have shown in our previous study with Mma20 infection in *tlr2*$^{-/-}$ zebrafish larvae [36]. Moreover, it has been demonstrated that mice deficient in TLR2 show increased susceptibility to *M. tuberculosis* infection [67, 68]. In agreement, Feng et al. reported that *Tlr2*$^{-/-}$ mice showed increased susceptibility to *M. avium*-infection compared with their wild type counterparts [69]. Interestingly, the bacterial growth in *Myd88*$^{-/-}$ mice infected with *M. avium* far exceeded that of *Tlr2*$^{-/-}$ and C57BL/6 mice. *M. avium*-

infected *Myd88*$^{-/-}$ mice died at 9-14 weeks post infection [69]. In contrast, no pronounced difference was observed in *M. avium*-infected *Tlr4*$^{-/-}$ mice and infected C57BL/6 mice [69]. In addition, TLR2 plays a role in active macrophages by recognition of *M. avium* biofilms on their surface [70]. Sweet et al. showed that TLR2 and MyD88, but not TLR4, activate macrophages through the glycopeptidolipids (GPLs) expressed on the surface of *M. avium* that are related to biofilm formation [70]. The studies suggest that TLR2, but not TLR4, plays a crucial protective role in mycobacterial infection. However, TLR2 is not the only member from the Toll-like receptor family that can respond to *M. avium* infection and trigger an immune response. TLR6 and TLR9 have also been shown to be required to effectively control *M. avium* growth in mice [71, 72]. In this study, we found that *tlr5a* and *tlr5b* were significantly upregulated in response to both *M. marinum* Mma20 and *M. avium* MAC 101 infection, while *myd88* was only significantly upregulated in the *M. avium* infection group (Fig. S2). It indicates that *tlr5a* and *tlr5b* are also involved in the process of the host response to *M. avium* infection and the role of *myd88* may be very important in this process. The function of *myd88*, *tlr5a*, and *tlr5b* in the NTM infection process are very interesting to be further investigated.

Tlr2 functions in defense against different mycobacterial species by regulating leukocyte cell migration

Although *tlr2* plays a protective role in the host defense against different NTM species, the underlying mechanisms may be different in infections by different mycobacterial species. We observed higher MAC 101 burdens inside *tlr2*$^{-/-}$ macrophages compared to *tlr2*$^{+/+}$ macrophages. This suggests that the bacterial clearance ability is impaired in the *tlr2* mutant upon MAC 101 infection. The antimicrobial function of TLR2 in macrophages has been previously demonstrated. In both mouse and human macrophages, the clearance of intracellular *M. tuberculosis* bacteria is dependent on TLR2 activation, although the mechanism of the antimicrobial activity is distinct between mouse and human macrophages [73]. In mouse macrophages, direct antimicrobial activity triggered by TLR2 is nitric oxide-dependent, however, this process is nitric oxide-independent in human macrophages [73, 74]. Liu et al. reported that human macrophage activation by TLR2 is related to vitamin D levels, which sustains the production of the antimicrobial peptide cathelicidin and subsequently leads to killing of intracellular tubercle bacilli [74]. In accordance, genes associated with the vitamin D receptor pathway are upregulated in wild type zebrafish larvae while they are downregulated in *tlr2* mutant after *M. marinum* infection [36]. This suggests that the higher susceptibility of the

tlr2 mutant to *M. marinum* and *M. avium* infection may be caused by impaired antimicrobial capacity of macrophages. Our observations of higher intracellular *M. avium* burdens in the *tlr2* mutants also supports this suggestion. The absence of differences in the intracellular bacterial burden found in *tlr2* mutant zebrafish after infection with *M. marinum* may have been caused by quicker death of infected macrophages in *M. marinum*-infected larvae. This hypothesis needs to be further validated.

Different mechanisms of *tlr2*-mediated defense against different mycobacterial species are apparently manifested in different effects on leukocyte behavior. In this study, we found that both macrophages and neutrophils moved faster in *tlr2* wild type larvae than in *tlr2* mutants after Mma20 infection, while *tlr2* deficiency did not affect neutrophil migration in MAC 101 infection. The meandering index of *tlr2* mutant macrophages was lower than the *tlr2* wild type macrophages in MAC 101 infection (Fig. 8). This altered leukocyte behavior suggests that chemokine expression profiles may be different in *tlr2* mutant zebrafish after infection by mycobacterial species. We previously reported that the expression levels of *cxcl11aa* and *cxcll11ac* after Mm infection was higher in 4 dpi *tlr2*$^{+/-}$ compared to 4 dpi *tlr2*$^{-/-}$ mutant zebrafish larvae [36]. Here we show that the chemokine gene expression profiles are different between the larvae infected with Mma20 and MAC 101 at the late infection stage in this study (Fig. 4). In future research we would like to investigate whether these differences in expression profiles can also be observed in the initial infection stage.

Materials and Methods

Zebrafish husbandry

The husbandry of adult zebrafish lines and all zebrafish experiments described in this study was in accordance with guidelines from the local animal welfare committee (DEC) of the university (License number: protocol 14,198), in compliance with the international guidelines specified by the EU Animal Protection Directive 2010/63/EU, and was conducted according to standard protocols (www.zfin.org). There was no adult zebrafish sacrificed in this study. All experiments were done with zebrafish larvae developed within 5 days post fertilization (dpf), therefore prior to the free-feeding stage and did not fall under animal experimentation law according to the EU Animal Protection Directive 2010/63/EU. Zebrafish eggs and larvae were cultured and grown at 28.5◦C in egg water (60 g/ml Instant Ocean sea salts). Zebrafish larvae were anesthetized

with egg water containing 0.02% buffered 3-aminobenzoic acid ethyl ester (Tricaine, Sigma-Aldrich, Netherlands) for bacterial infection and imaging experiments.

The ABTL wild type zebrafish strain, *tlr2*^{sa19423} mutant (ENU-mutagenized) and its wild type siblings or the following transgenic lines: *Tg (Mpeg1:EGFP)*^{gl22}, *tlr2*$^{+/+}$ *Tg (mpeg1:mCherry-F);TgBAC (mpx: EGFP)* and *tlr2*$^{-/-}$ *Tg (mpeg1:mCherry-F);TgBAC (mpx: EGFP)* were used for this study [29, 36].

Bacterial strain culture

The *Mycobacterium marinum* m20 (Mma20), the *Mycobacterium avium Chester* (also called MAC 101, ATCC® 700898™), Mma20 expressing mCherry fluorescent protein [23], MAC 101 containing the Wasabi expression vector pSMT3 (Addgene, plasmid 26589), and MAC 101 expressing DsRed through pND239 plasmid [75] were used in this study to induce infection in zebrafish embryos. The Mma20 and MAC 101 without any fluorescent protein were grown at 28.5◦C in Middlebrook 7H9 broth with acid-albumin-dextrose-catalase (ADC) enrichment or Middlebrook 7H10 agar with 10% oleic acid-albumin-dextrose-catalase (OADC) enrichment. The Mma20 mCherry, MAC 101 Wasabi and MAC 101 DsRed were grown in the same medium or plates with hygromycin 50 µg/mL.

Alexa Fluor dye staining of mycobacteria

To visualize the interaction between the mycobacteria and leukocytes, the succinimidyl esters (NHS ester) of Alexa Fluor 647 (Invitrogen, A20006) was applied to stain the mycobacteria. The dye was dissolved in high-quality, anhydrous dimethylsulfoxide (DMSO) at a final concentration of 5 mg/mL for preparing the reactive dye solution. For this method, Mma20 and MAC101 were cultured in 7H9 broth based on the description above and were harvest in their logarithmic phase. The mycobacterial strains were re-suspended in 250 µL 0.1 M sodium bicarbonate buffer ($NaHCO_3$, pH 8.3) and then slowly added 10 µL of the reactive dye solution. The mixture was incubated at room temperature for 20 min. Subsequently, the stained mycobacteria were washed twice by sterile PBS. The Alexa Fluor strained Mma20 and MAC101 were used for the cell tracking and the cell recruitment assay.

Microinjection

Liquid cultures of Mma20 and MAC 101 were harvested and prepared for the microinjection, according to procedures described before in [76]. In short, mycobacterial strains were grown to

the logarithmic phase and harvested by centrifugation and washing three times in sterile PBS. Subsequently, bacterial suspensions were re-suspended in sterile PBS with 2% polyvinylpyrrolidone (PVP40) with the desired concentration by measuring the OD600. An OD600 of 1 corresponds to approximately 10^8 MAC 101, which is the same as Mma20 (data are not shown). Embryos were systemically infected with ~150 CFU mCherry-labeled Mma20 or Wasabi-labeled ~4500 CFU MAC 101 through blood island infection at 28 hpf by using the method described in [76]. For quantification of the bacterial burden, we analyzed the correlation between MAC 101 CFU and average fluorescent signal (Fig. S5). To observe macrophage and neutrophil migration behavior upon mycobacterial infection, zebrafish tailfin infection model was applied [37, 41]. Zebrafish larvae were locally infected in the tail fin at 3 dpf with ~50 CFU Mma20 or MAC 101 as previously described [37, 41].

Imaging and quantification of bacterial burden

Mycobacterial infected ABTL, *tlr2*$^{+/+}$, and *tlr2*$^{-/-}$ zebrafish larvae were imaged at 1 dpi and 4 dpi for the quantification of the bacterial burden changes by using a Leica M205FA fluorescence stereomicroscope, equipped with a Leica DFC 345FX camera. All experiments were performed three times independently and in the same microscope setting. The integrated intensity of bacterial loads was quantified by using Quantifish software (https://github.com/DavidStirling/QuantiFish) [77].

Confocal microscopy imaging

Confocal microscopy imaging was applied for the observation of the granuloma-like cluster and the investigation of the leukocyte migration behavior upon two mycobacterial infections. Observed larvae for each condition were embedded in 1% low melting point agarose (Sigma Aldrich) with 0.02% tricaine and imaged under a Leica TCS SP8 confocal microscope (Leica Microsystems). 4 dpi blood island infected larvae or 3 dpi tail fin infected larvae were imaged with a 20× objective (N.A. 0.75) or a 40× objective (N.A. oil immersion, N.A. 1.3) to observe the phenotype of the granuloma-like clusters upon two different mycobacterial infections. In order to investigate the leukocyte migration behavior upon two mycobacterial infections, living imaging was performed on 1 hpi tail fin infected larvae with a 1 min time interval for 2 h imaging using a 20× objective (N.A. 0.75). Acquisition settings for the living imaging were kept the same across the groups.

RNA isolation, deep sequencing and data analysis

To compare the difference of the larvae infected with *M. marinum* Mma20 infection or *M. avium* MAC 101 infection, the RNAseq data of 4 dpi zebrafish larvae infected with ~250 CFU Mma20 was used (GEO database accession for the RNASeq data: GSE76499) [32]. Fifteen 4 dpi ABTL wild type larvae infected with ~4500 CFU MAC 101 (three replicates) were collected for the total RNA isolation. The same amount of ABTL wild type larvae (three replicates) were injected with sterile PBS as a control group. The total RNAs were isolated by using TRIzol Reagent (Life Technologies) to create RNAseq libraries. Moreover, DNase treatment (Thermo Fisher Scientific, EN0525) was applied to eliminate the effect of the DNA from the samples following the manufacturer's instructions. The concentration and quality of RNAs were assessed by NanoDrop 2000 (Thermo Fisher Scientific, the Netherlands).

The deep sequencing was performed in the company GenomeScan (GenomeScan B. V., Plesmanlaan 1d, 2333 BZ, Leiden, Netherlands). The RNAseq libraries were sequenced by applying a NovaSeq 6000 v1.5 device. Image analysis, base calling, and quality check were done by the Illumina data analysis pipeline RTA3.4.4 and Bclfastq v2.20. Subsequently, RNAseq reads were aligned against the zebrafish genome (GRCz11) by using CLC genomic workbench software (QIAGEN, Cat. 832583). The percent of aligned reads mapping is exceeding 90% among all samples in this study.

The Differential Expression in Two Groups tool from the CLC genomic workbench was used to acquire the differential expressed genes (DEGs) between the mycobacterial infection and its control groups. In brief, the tool performs a statistical differential expression test based on a negative binomial Generalized Linear Model (GLM) (See the user manual of the CLC genomic workbench, page 829: https://resources.qiagenbioinformatics.com/manuals/clcgenomicsworkbench/current/User_Manual.pdf) [78]. The output data were used for further analysis. A cut-oof setting of the FDR p-value < 0.05 and |FoldChange| > 2 was used to define significantly regulated DEGs. Pathvisio 3.3.0 (https://pathvisio.github.io/downloads) was applied for the visualization of the significantly regulated genes in the pathways [79].

Cell tracking and its quantification

The 4D files of leukocyte tracking generated from time-lapse acquisitions were processed by using Imaris x64 7.4 (Bitplane) or ImageJ (NIH, Bethesda, ML, USA). An automatic 3D cell

tracking algorithm in Imaris x64 7.4 (Bitplane) was employed to build macrophage or neutrophil trajectories in the living imaging of mycobacterial infected larvae. The data of the number, mean speed, and meandering index of recruited leukocytes in the infected tail fin region were output from the Imaris software. To confirm the results from the Imaris software, another automatic 3D cell tracking plug-in, 3D Track Foci, was applied [43]. The overall mean speed of macrophages or neutrophils was calculated using the 3D Track Foci for each larva.

Statistical analyses

The statistical analysis of Fig. 1, 5, 6, 8, 9, and Fig. S3 was done by using Graphpad Prism software (Version 9.0.0; GraphPad Software, San Diego, CA, USA). All experiment data in this study are shown as mean ± SD. D' Agostino-Pearson omnibus normality test was performed to determine the normal (Guassian) distribution of the data and unpaired two-tailed t-tests were applied. A parametric test was carried out when the data meets the normal distribution, otherwise the Mann-Whitney test which is a nonparametric test was used. Significance was established at $P < 0.05$ and the other significance levels are indicated as * $P < 0.05$; ** $P < 0.01$; *** $P < 0.001$; **** $P < 0.0001$.

Acknowledgments

This work was supported by a grant from the Innovative Medicines Initiative 2 Joint Undertaking (IMI2 JU) under the RespiriNTM project (Grant No. 853932). We would like to thank our colleagues from Leiden University: Mariëlle C. Haks and Gül Kilinç for supplying us with the pSTM3 Wasabi plasmid, Gerda E.M. Lamers for assistance with confocal laser scanning imaging and Joost J. Willemse for providing microscopic analysis programs. We thank all members of the fish facility team for fish caretaking.

References

1. Hoefsloot W, van Ingen J, Andrejak C, Angeby K, Bauriaud R, Bemer P, et al. The geographic diversity of nontuberculous mycobacteria isolated from pulmonary samples: an NTM-NET collaborative study. Eur Respir J. 2013;42(6):1604-13. Epub 2013/04/20. doi: 10.1183/09031936.00149212. PubMed PMID: 23598956.

2. Nishiuchi Y, Iwamoto T, Maruyama F. Infection Sources of a Common Non-tuberculous Mycobacterial Pathogen, Mycobacterium avium Complex. Front Med (Lausanne). 2017;4:27. Epub 2017/03/23. doi: 10.3389/fmed.2017.00027. PubMed PMID: 28326308; PubMed Central PMCID: PMCPMC5339636.

3. Tortoli E. Microbiological features and clinical relevance of new species of the genus Mycobacterium. Clin Microbiol Rev. 2014;27(4):727-52. Epub 2014/10/04. doi: 10.1128/CMR.00035-14. PubMed PMID: 25278573; PubMed Central PMCID: PMCPMC4187642.

4. Saxena S, Spaink HP, Forn-Cuni G. Drug Resistance in Nontuberculous Mycobacteria: Mechanisms and Models. Biology (Basel). 2021;10(2). Epub 2021/02/13. doi: 10.3390/biology10020096. PubMed PMID: 33573039; PubMed Central PMCID: PMCPMC7911849.

5. Kilinc G, Saris A, Ottenhoff THM, Haks MC. Host-directed therapy to combat mycobacterial infections. Immunol Rev. 2021. Epub 2021/02/11. doi: 10.1111/imr.12951. PubMed PMID: 33565103.

6. Strong EJ, Lee S. Targeting Autophagy as a Strategy for Developing New Vaccines and Host-Directed Therapeutics Against Mycobacteria. Front Microbiol. 2020;11:614313. Epub 2021/02/02. doi: 10.3389/fmicb.2020.614313. PubMed PMID: 33519771; PubMed Central PMCID: PMCPMC7840607.

7. Tomioka H, Sano C, Tatano Y. Host-Directed Therapeutics against Mycobacterial Infections. Curr Pharm Des. 2017;23(18):2644-56. Epub 2016/12/03. doi: 10.2174/1381612822666161202121550. PubMed PMID: 27908271.

8. Inderlied CB, Kemper CA, Bermudez LE. The Mycobacterium avium complex. Clin Microbiol Rev. 1993;6(3):266-310. Epub 1993/07/01. doi: 10.1128/cmr.6.3.266. PubMed PMID: 8358707; PubMed Central PMCID: PMCPMC358286.

9. Griffith DE, Aksamit T, Brown-Elliott BA, Catanzaro A, Daley C, Gordin F, et al. An official ATS/IDSA statement: diagnosis, treatment, and prevention of nontuberculous mycobacterial diseases. Am J Respir Crit Care Med. 2007;175(4):367-416. Epub 2007/02/06. doi: 10.1164/rccm.200604-571ST. PubMed PMID: 17277290.

10. Lam PK, Griffith DE, Aksamit TR, Ruoss SJ, Garay SM, Daley CL, et al. Factors related to response to intermittent treatment of Mycobacterium avium complex lung disease. Am J Respir Crit Care Med. 2006;173(11):1283-9. Epub 2006/03/04. doi: 10.1164/rccm.200509-1531OC. PubMed PMID: 16514112.

11. Park SW, Song JW, Shim TS, Park MS, Lee HL, Uh ST, et al. Mycobacterial pulmonary infections in patients with idiopathic pulmonary fibrosis. J Korean Med Sci. 2012;27(8):896-900. Epub 2012/08/10. doi: 10.3346/jkms.2012.27.8.896. PubMed PMID: 22876056; PubMed Central PMCID: PMCPMC3410237.

12. Verma D, Chan ED, Ordway DJ. The double-edged sword of Tregs in M tuberculosis, M avium, and M absessus infection. Immunol Rev. 2021. Epub 2021/03/14. doi: 10.1111/imr.12959. PubMed PMID: 33713043.

13. Bohlson SS, Strasser JA, Bower JJ, Schorey JS. Role of complement in Mycobacterium avium pathogenesis: in vivo and in vitro analyses of the host response to infection in the absence of complement component C3. Infect Immun. 2001;69(12):7729-35. Epub 2001/11/14. doi: 10.1128/IAI.69.12.7729-7735.2001. PubMed PMID: 11705954; PubMed Central PMCID: PMCPMC98868.

14. Irani VR, Maslow JN. Induction of murine macrophage TNF-alpha synthesis by Mycobacterium avium is modulated through complement-dependent interaction via complement receptors 3 and 4 in relation to M. avium glycopeptidolipid. FEMS Microbiol Lett. 2005;246(2):221-8. Epub 2005/05/19. doi: 10.1016/j.femsle.2005.04.008. PubMed PMID: 15899409.

15. Shin MK, Shin SJ. Genetic Involvement of Mycobacterium avium Complex in the Regulation and Manipulation of Innate Immune Functions of Host Cells. Int J Mol Sci. 2021;22(6). Epub 2021/04/04. doi: 10.3390/ijms22063011. PubMed PMID: 33809463; PubMed Central PMCID: PMCPMC8000623.

16. Shin JI, Shin SJ, Shin MK. Differential Genotyping of Mycobacterium avium Complex and Its Implications in Clinical and Environmental Epidemiology. Microorganisms. 2020;8(1). Epub 2020/01/16. doi: 10.3390/microorganisms8010098. PubMed PMID: 31936743; PubMed Central PMCID: PMCPMC7022546.
17. Andrejak C, Almeida DV, Tyagi S, Converse PJ, Ammerman NC, Grosset JH. Characterization of mouse models of Mycobacterium avium complex infection and evaluation of drug combinations. Antimicrob Agents Chemother. 2015;59(4):2129-35. Epub 2015/01/28. doi: 10.1128/AAC.04841-14. PubMed PMID: 25624335; PubMed Central PMCID: PMCPMC4356827.
18. Gangadharam PR, Perumal VK, Farhi DC, LaBrecque J. The beige mouse model for Mycobacterium avium complex (MAC) disease: optimal conditions for the host and parasite. Tubercle. 1989;70(4):257-71. Epub 1989/12/01. doi: 10.1016/0041-3879(89)90020-2. PubMed PMID: 2626803.
19. Torraca V, Masud S, Spaink HP, Meijer AH. Macrophage-pathogen interactions in infectious diseases: new therapeutic insights from the zebrafish host model. Dis Model Mech. 2014;7(7):785-97. Epub 2014/06/29. doi: 10.1242/dmm.015594. PubMed PMID: 24973749; PubMed Central PMCID: PMCPMC4073269.
20. Tobin DM, May RC, Wheeler RT. Zebrafish: a see-through host and a fluorescent toolbox to probe host-pathogen interaction. PLoS Pathog. 2012;8(1):e1002349. Epub 2012/01/14. doi: 10.1371/journal.ppat.1002349. PubMed PMID: 22241986; PubMed Central PMCID: PMCPMC3252360.
21. Meijer AH, Spaink HP. Host-pathogen interactions made transparent with the zebrafish model. Curr Drug Targets. 2011;12(7):1000-17. Epub 2011/03/04. doi: 10.2174/138945011795677809. PubMed PMID: 21366518; PubMed Central PMCID: PMCPMC3319919.
22. Meijer AH. Protection and pathology in TB: learning from the zebrafish model. Semin Immunopathol. 2016;38(2):261-73. Epub 2015/09/02. doi: 10.1007/s00281-015-0522-4. PubMed PMID: 26324465; PubMed Central PMCID: PMCPMC4779130.
23. van der Sar AM, Spaink HP, Zakrzewska A, Bitter W, Meijer AH. Specificity of the zebrafish host transcriptome response to acute and chronic mycobacterial infection and the role of innate and adaptive immune components. Mol Immunol. 2009;46(11-12):2317-32. Epub 2009/05/05. doi: 10.1016/j.molimm.2009.03.024. PubMed PMID: 19409617.
24. Hato T, Dagher PC. How the Innate Immune System Senses Trouble and Causes Trouble. Clin J Am Soc Nephrol. 2015;10(8):1459-69. Epub 2014/11/22. doi: 10.2215/CJN.04680514. PubMed PMID: 25414319; PubMed Central PMCID: PMCPMC4527020.
25. Oliveira-Nascimento L, Massari P, Wetzler LM. The Role of TLR2 in Infection and Immunity. Front Immunol. 2012;3:79. Epub 2012/05/09. doi: 10.3389/fimmu.2012.00079. PubMed PMID: 22566960; PubMed Central PMCID: PMCPMC3342043.
26. Mukherjee S, Karmakar S, Babu SP. TLR2 and TLR4 mediated host immune responses in major infectious diseases: a review. Braz J Infect Dis. 2016;20(2):193-204. Epub 2016/01/19. doi: 10.1016/j.bjid.2015.10.011. PubMed PMID: 26775799.
27. Uematsu S, Akira S. Toll-Like receptors (TLRs) and their ligands. Handb Exp Pharmacol. 2008;(183):1-20. Epub 2007/12/12. doi: 10.1007/978-3-540-72167-3_1. PubMed PMID: 18071652.
28. Tjarnlund A, Guirado E, Julian E, Cardona PJ, Fernandez C. Determinant role for Toll-like receptor signalling in acute mycobacterial infection in the respiratory tract. Microbes Infect. 2006;8(7):1790-800. Epub 2006/07/04. doi: 10.1016/j.micinf.2006.02.017. PubMed PMID: 16815067.

29. Hu W, van Steijn L, Li C, Verbeek FJ, Cao L, Merks RMH, et al. A Novel Function of TLR2 and MyD88 in the Regulation of Leukocyte Cell Migration Behavior During Wounding in Zebrafish Larvae. Front Cell Dev Biol. 2021;9:624571. Epub 2021/03/05. doi: 10.3389/fcell.2021.624571. PubMed PMID: 33659250; PubMed Central PMCID: PMCPMC7917198.

30. Simpson ME, Petri WA, Jr. TLR2 as a Therapeutic Target in Bacterial Infection. Trends Mol Med. 2020;26(8):715-7. Epub 2020/06/22. doi: 10.1016/j.molmed.2020.05.006. PubMed PMID: 32563557; PubMed Central PMCID: PMCPMC7845793.

31. Davis JM, Clay H, Lewis JL, Ghori N, Herbomel P, Ramakrishnan L. Real-time visualization of mycobacterium-macrophage interactions leading to initiation of granuloma formation in zebrafish embryos. Immunity. 2002;17(6):693-702. Epub 2002/12/14. doi: 10.1016/s1074-7613(02)00475-2. PubMed PMID: 12479816.

32. Benard EL, Rougeot J, Racz PI, Spaink HP, Meijer AH. Transcriptomic Approaches in the Zebrafish Model for Tuberculosis-Insights Into Host- and Pathogen-specific Determinants of the Innate Immune Response. Adv Genet. 2016;95:217-51. Epub 2016/08/10. doi: 10.1016/bs.adgen.2016.04.004. PubMed PMID: 27503359.

33. Ryffel B, Jacobs M, Parida S, Botha T, Togbe D, Quesniaux V. Toll-like receptors and control of mycobacterial infection in mice. Novartis Found Symp. 2006;279:127-39; discussion 39-41, 216-9. Epub 2007/02/07. PubMed PMID: 17278391.

34. Heldwein KA, Fenton MJ. The role of Toll-like receptors in immunity against mycobacterial infection. Microbes Infect. 2002;4(9):937-44. Epub 2002/07/11. doi: 10.1016/s1286-4579(02)01611-8. PubMed PMID: 12106786.

35. Vu A, Calzadilla A, Gidfar S, Calderon-Candelario R, Mirsaeidi M. Toll-like receptors in mycobacterial infection. Eur J Pharmacol. 2017;808:1-7. Epub 2016/10/30. doi: 10.1016/j.ejphar.2016.10.018. PubMed PMID: 27756604.

36. Hu W, Yang S, Shimada Y, Munch M, Marin-Juez R, Meijer AH, et al. Infection and RNA-seq analysis of a zebrafish tlr2 mutant shows a broad function of this toll-like receptor in transcriptional and metabolic control and defense to Mycobacterium marinum infection. BMC Genomics. 2019;20(1):878. Epub 2019/11/22. doi: 10.1186/s12864-019-6265-1. PubMed PMID: 31747871; PubMed Central PMCID: PMCPMC6869251.

37. Hosseini R, Lamers GE, Soltani HM, Meijer AH, Spaink HP, Schaaf MJ. Efferocytosis and extrusion of leukocytes determine the progression of early mycobacterial pathogenesis. J Cell Sci. 2016;129(18):3385-95. Epub 2016/07/30. doi: 10.1242/jcs.135194. PubMed PMID: 27469488.

38. Clay H, Davis JM, Beery D, Huttenlocher A, Lyons SE, Ramakrishnan L. Dichotomous role of the macrophage in early Mycobacterium marinum infection of the zebrafish. Cell Host Microbe. 2007;2(1):29-39. Epub 2007/11/17. doi: 10.1016/j.chom.2007.06.004. PubMed PMID: 18005715; PubMed Central PMCID: PMCPMC3115716.

39. Yang CT, Cambier CJ, Davis JM, Hall CJ, Crosier PS, Ramakrishnan L. Neutrophils exert protection in the early tuberculous granuloma by oxidative killing of mycobacteria phagocytosed from infected macrophages. Cell Host Microbe. 2012;12(3):301-12. Epub 2012/09/18. doi: 10.1016/j.chom.2012.07.009. PubMed PMID: 22980327; PubMed Central PMCID: PMCPMC3638950.

40. Bernut A, Nguyen-Chi M, Halloum I, Herrmann JL, Lutfalla G, Kremer L. Mycobacterium abscessus-Induced Granuloma Formation Is Strictly Dependent on TNF Signaling and Neutrophil Trafficking. PLoS

Pathog. 2016;12(11):e1005986. Epub 2016/11/03. doi: 10.1371/journal.ppat.1005986. PubMed PMID: 27806130; PubMed Central PMCID: PMCPMC5091842.

41. Hosseini R, Lamers GE, Hodzic Z, Meijer AH, Schaaf MJ, Spaink HP. Correlative light and electron microscopy imaging of autophagy in a zebrafish infection model. Autophagy. 2014;10(10):1844-57. Epub 2014/08/16. doi: 10.4161/auto.29992. PubMed PMID: 25126731; PubMed Central PMCID: PMCPMC4198367.

42. Kimmel CB, Ballard WW, Kimmel SR, Ullmann B, Schilling TF. Stages of embryonic development of the zebrafish. Dev Dyn. 1995;203(3):253-310. Epub 1995/07/01. doi: 10.1002/aja.1002030302. PubMed PMID: 8589427.

43. Celler K, van Wezel GP, Willemse J. Single particle tracking of dynamically localizing TatA complexes in Streptomyces coelicolor. Biochem Biophys Res Commun. 2013;438(1):38-42. Epub 2013/07/23. doi: 10.1016/j.bbrc.2013.07.016. PubMed PMID: 23867823.

44. Prevots DR, Marras TK. Epidemiology of human pulmonary infection with nontuberculous mycobacteria: a review. Clin Chest Med. 2015;36(1):13-34. Epub 2015/02/14. doi: 10.1016/j.ccm.2014.10.002. PubMed PMID: 25676516; PubMed Central PMCID: PMCPMC4332564.

45. Nasiri MJ, Calcagno T, Hosseini SS, Hematian A, Nojookambari NY, Karimi-Yazdi M, et al. Role of Clofazimine in Treatment of Mycobacterium avium Complex. Front Med (Lausanne). 2021;8:638306. Epub 2021/05/11. doi: 10.3389/fmed.2021.638306. PubMed PMID: 33968952; PubMed Central PMCID: PMCPMC8099105.

46. Prevots DR, Shaw PA, Strickland D, Jackson LA, Raebel MA, Blosky MA, et al. Nontuberculous mycobacterial lung disease prevalence at four integrated health care delivery systems. Am J Respir Crit Care Med. 2010;182(7):970-6. Epub 2010/06/12. doi: 10.1164/rccm.201002-0310OC. PubMed PMID: 20538958; PubMed Central PMCID: PMCPMC2970866.

47. Tonjum T, Welty DB, Jantzen E, Small PL. Differentiation of Mycobacterium ulcerans, M. marinum, and M. haemophilum: mapping of their relationships to M. tuberculosis by fatty acid profile analysis, DNA-DNA hybridization, and 16S rRNA gene sequence analysis. J Clin Microbiol. 1998;36(4):918-25. Epub 1998/05/23. doi: 10.1128/JCM.36.4.918-925.1998. PubMed PMID: 9542909; PubMed Central PMCID: PMCPMC104661.

48. Weiss G, Schaible UE. Macrophage defense mechanisms against intracellular bacteria. Immunol Rev. 2015;264(1):182-203. Epub 2015/02/24. doi: 10.1111/imr.12266. PubMed PMID: 25703560; PubMed Central PMCID: PMCPMC4368383.

49. Pagan AJ, Yang CT, Cameron J, Swaim LE, Ellett F, Lieschke GJ, et al. Myeloid Growth Factors Promote Resistance to Mycobacterial Infection by Curtailing Granuloma Necrosis through Macrophage Replenishment. Cell Host Microbe. 2015;18(1):15-26. Epub 2015/07/15. doi: 10.1016/j.chom.2015.06.008. PubMed PMID: 26159717; PubMed Central PMCID: PMCPMC4509513.

50. Tobin DM, Vary JC, Jr., Ray JP, Walsh GS, Dunstan SJ, Bang ND, et al. The lta4h locus modulates susceptibility to mycobacterial infection in zebrafish and humans. Cell. 2010;140(5):717-30. Epub 2010/03/10. doi: 10.1016/j.cell.2010.02.013. PubMed PMID: 20211140; PubMed Central PMCID: PMCPMC2907082.

51. Grosset J. Mycobacterium tuberculosis in the extracellular compartment: an underestimated adversary. Antimicrob Agents Chemother. 2003;47(3):833-6. Epub 2003/02/27. doi: 10.1128/AAC.47.3.833-836.2003. PubMed PMID: 12604509; PubMed Central PMCID: PMCPMC149338.

52. Bernut A, Herrmann JL, Kissa K, Dubremetz JF, Gaillard JL, Lutfalla G, et al. Mycobacterium abscessus cording prevents phagocytosis and promotes abscess formation. Proc Natl Acad Sci U S A. 2014;111(10):E943-52. Epub 2014/02/26. doi: 10.1073/pnas.1321390111. PubMed PMID: 24567393; PubMed Central PMCID: PMCPMC3956181.

53. Johansen MD, Kremer L. CFTR Depletion Confers Hypersusceptibility to Mycobacterium fortuitum in a Zebrafish Model. Front Cell Infect Microbiol. 2020;10:357. Epub 2020/08/28. doi: 10.3389/fcimb.2020.00357. PubMed PMID: 32850470; PubMed Central PMCID: PMCPMC7396536.

54. Olson G, McNulty MC, Mullane K, Beavis KG, Tesic V. Cording in Disseminated Mycobacterium chelonae Infection in an Immunocompromised Patient. Lab Med. 2021;52(3):e50-e2. Epub 2020/09/22. doi: 10.1093/labmed/lmaa082. PubMed PMID: 32954440.

55. Hybiske K, Stephens RS. Exit strategies of intracellular pathogens. Nat Rev Microbiol. 2008;6(2):99-110. Epub 2008/01/17. doi: 10.1038/nrmicro1821. PubMed PMID: 18197167.

56. Awuh JA, Flo TH. Molecular basis of mycobacterial survival in macrophages. Cell Mol Life Sci. 2017;74(9):1625-48. Epub 2016/11/21. doi: 10.1007/s00018-016-2422-8. PubMed PMID: 27866220.

57. Ufimtseva E. Mycobacterium-Host Cell Relationships in Granulomatous Lesions in a Mouse Model of Latent Tuberculous Infection. Biomed Res Int. 2015;2015:948131. Epub 2015/06/13. doi: 10.1155/2015/948131. PubMed PMID: 26064970; PubMed Central PMCID: PMCPMC4433666.

58. Cowley S. The biology of HIV infection. Lepr Rev. 2001;72(2):212-20. Epub 2001/08/10. doi: 10.5935/0305-7518.20010028. PubMed PMID: 11495453.

59. Katkoori VR, Basson MD, Bond VC, Manne U, Bumpers HL. Nef-M1, a peptide antagonist of CXCR4, inhibits tumor angiogenesis and epithelialtomesenchymal transition in colon and breast cancers. Oncotarget. 2015;6(29):27763-77. Epub 2015/09/01. doi: 10.18632/oncotarget.4615. PubMed PMID: 26318034; PubMed Central PMCID: PMCPMC4695024.

60. Torraca V, Tulotta C, Snaar-Jagalska BE, Meijer AH. The chemokine receptor CXCR4 promotes granuloma formation by sustaining a mycobacteria-induced angiogenesis programme. Sci Rep. 2017;7:45061. Epub 2017/03/24. doi: 10.1038/srep45061. PubMed PMID: 28332618; PubMed Central PMCID: PMCPMC5362882.

61. Doncker AV, Balabanian K, Bellanne-Chantelot C, de Guibert S, Revest M, Bachelerie F, et al. Two cases of disseminated Mycobacterium avium infection associated with a new immunodeficiency syndrome related to CXCR4 dysfunctions. Clin Microbiol Infect. 2011;17(2):135-9. Epub 2010/02/13. doi: 10.1111/j.1469-0691.2010.03187.x. PubMed PMID: 20148920.

62. Link DC. Neutrophil homeostasis: a new role for stromal cell-derived factor-1. Immunol Res. 2005;32(1-3):169-78. Epub 2005/08/18. doi: 10.1385/IR:32:1-3:169. PubMed PMID: 16106067.

63. Torraca V, Cui C, Boland R, Bebelman JP, van der Sar AM, Smit MJ, et al. The CXCR3-CXCL11 signaling axis mediates macrophage recruitment and dissemination of mycobacterial infection. Dis Model Mech. 2015;8(3):253-69. Epub 2015/01/13. doi: 10.1242/dmm.017756. PubMed PMID: 25573892; PubMed Central PMCID: PMCPMC4348563.

64. Roecklein JA, Swartz RP, Yeager H, Jr. Nonopsonic uptake of Mycobacterium avium complex by human monocytes and alveolar macrophages. J Lab Clin Med. 1992;119(6):772-81. Epub 1992/06/11. PubMed PMID: 1593222.

65. Schorey JS, Carroll MC, Brown EJ. A macrophage invasion mechanism of pathogenic mycobacteria. Science. 1997;277(5329):1091-3. Epub 1997/08/22. doi: 10.1126/science.277.5329.1091. PubMed PMID: 9262476.

66. Mold C. Role of complement in host defense against bacterial infection. Microbes Infect. 1999;1(8):633-8. Epub 1999/12/28. doi: 10.1016/s1286-4579(99)80063-x. PubMed PMID: 10611740.

67. Reiling N, Holscher C, Fehrenbach A, Kroger S, Kirschning CJ, Goyert S, et al. Cutting edge: Toll-like receptor (TLR)2- and TLR4-mediated pathogen recognition in resistance to airborne infection with Mycobacterium tuberculosis. J Immunol. 2002;169(7):3480-4. Epub 2002/09/24. doi: 10.4049/jimmunol.169.7.3480. PubMed PMID: 12244136.

68. Drennan MB, Nicolle D, Quesniaux VJ, Jacobs M, Allie N, Mpagi J, et al. Toll-like receptor 2-deficient mice succumb to Mycobacterium tuberculosis infection. Am J Pathol. 2004;164(1):49-57. Epub 2003/12/26. doi: 10.1016/S0002-9440(10)63095-7. PubMed PMID: 14695318; PubMed Central PMCID: PMCPMC1602241.

69. Feng CG, Scanga CA, Collazo-Custodio CM, Cheever AW, Hieny S, Caspar P, et al. Mice lacking myeloid differentiation factor 88 display profound defects in host resistance and immune responses to Mycobacterium avium infection not exhibited by Toll-like receptor 2 (TLR2)- and TLR4-deficient animals. J Immunol. 2003;171(9):4758-64. Epub 2003/10/22. doi: 10.4049/jimmunol.171.9.4758. PubMed PMID: 14568952.

70. Sweet L, Schorey JS. Glycopeptidolipids from Mycobacterium avium promote macrophage activation in a TLR2- and MyD88-dependent manner. J Leukoc Biol. 2006;80(2):415-23. Epub 2006/06/09. doi: 10.1189/jlb.1205702. PubMed PMID: 16760377.

71. Marinho FA, de Paula RR, Mendes AC, de Almeida LA, Gomes MT, Carvalho NB, et al. Toll-like receptor 6 senses Mycobacterium avium and is required for efficient control of mycobacterial infection. Eur J Immunol. 2013;43(9):2373-85. Epub 2013/05/30. doi: 10.1002/eji.201243208. PubMed PMID: 23716075.

72. Carvalho NB, Oliveira FS, Duraes FV, de Almeida LA, Florido M, Prata LO, et al. Toll-like receptor 9 is required for full host resistance to Mycobacterium avium infection but plays no role in induction of Th1 responses. Infect Immun. 2011;79(4):1638-46. Epub 2011/02/09. doi: 10.1128/IAI.01030-10. PubMed PMID: 21300776; PubMed Central PMCID: PMCPMC3067546.

73. Thoma-Uszynski S, Stenger S, Takeuchi O, Ochoa MT, Engele M, Sieling PA, et al. Induction of direct antimicrobial activity through mammalian toll-like receptors. Science. 2001;291(5508):1544-7. Epub 2001/02/27. doi: 10.1126/science.291.5508.1544. PubMed PMID: 11222859.

74. Liu PT, Stenger S, Li H, Wenzel L, Tan BH, Krutzik SR, et al. Toll-like receptor triggering of a vitamin D-mediated human antimicrobial response. Science. 2006;311(5768):1770-3. Epub 2006/02/25. doi: 10.1126/science.1123933. PubMed PMID: 16497887.

75. Manina G, Dhar N, McKinney JD. Stress and host immunity amplify Mycobacterium tuberculosis phenotypic heterogeneity and induce nongrowing metabolically active forms. Cell Host Microbe. 2015;17(1):32-46. Epub 2014/12/30. doi: 10.1016/j.chom.2014.11.016. PubMed PMID: 25543231.

76. Benard EL, van der Sar AM, Ellett F, Lieschke GJ, Spaink HP, Meijer AH. Infection of zebrafish embryos with intracellular bacterial pathogens. J Vis Exp. 2012;(61). Epub 2012/03/29. doi: 10.3791/3781. PubMed PMID: 22453760; PubMed Central PMCID: PMCPMC3415172.

77. Stirling DR, Suleyman O, Gil E, Elks PM, Torraca V, Noursadeghi M, et al. Analysis tools to quantify dissemination of pathology in zebrafish larvae. Sci Rep. 2020;10(1):3149. Epub 2020/02/23. doi: 10.1038/s41598-020-59932-1. PubMed PMID: 32081863; PubMed Central PMCID: PMCPMC7035342.

78. McCarthy DJ, Chen Y, Smyth GK. Differential expression analysis of multifactor RNA-Seq experiments with respect to biological variation. Nucleic Acids Res. 2012;40(10):4288-97. Epub 2012/01/31. doi: 10.1093/nar/gks042. PubMed PMID: 22287627; PubMed Central PMCID: PMCPMC3378882.

79. Kutmon M, van Iersel MP, Bohler A, Kelder T, Nunes N, Pico AR, et al. PathVisio 3: an extendable pathway analysis toolbox. PLoS Comput Biol. 2015;11(2):e1004085. Epub 2015/02/24. doi: 10.1371/journal.pcbi.1004085. PubMed PMID: 25706687; PubMed Central PMCID: PMCPMC4338111.

Supplementary materials

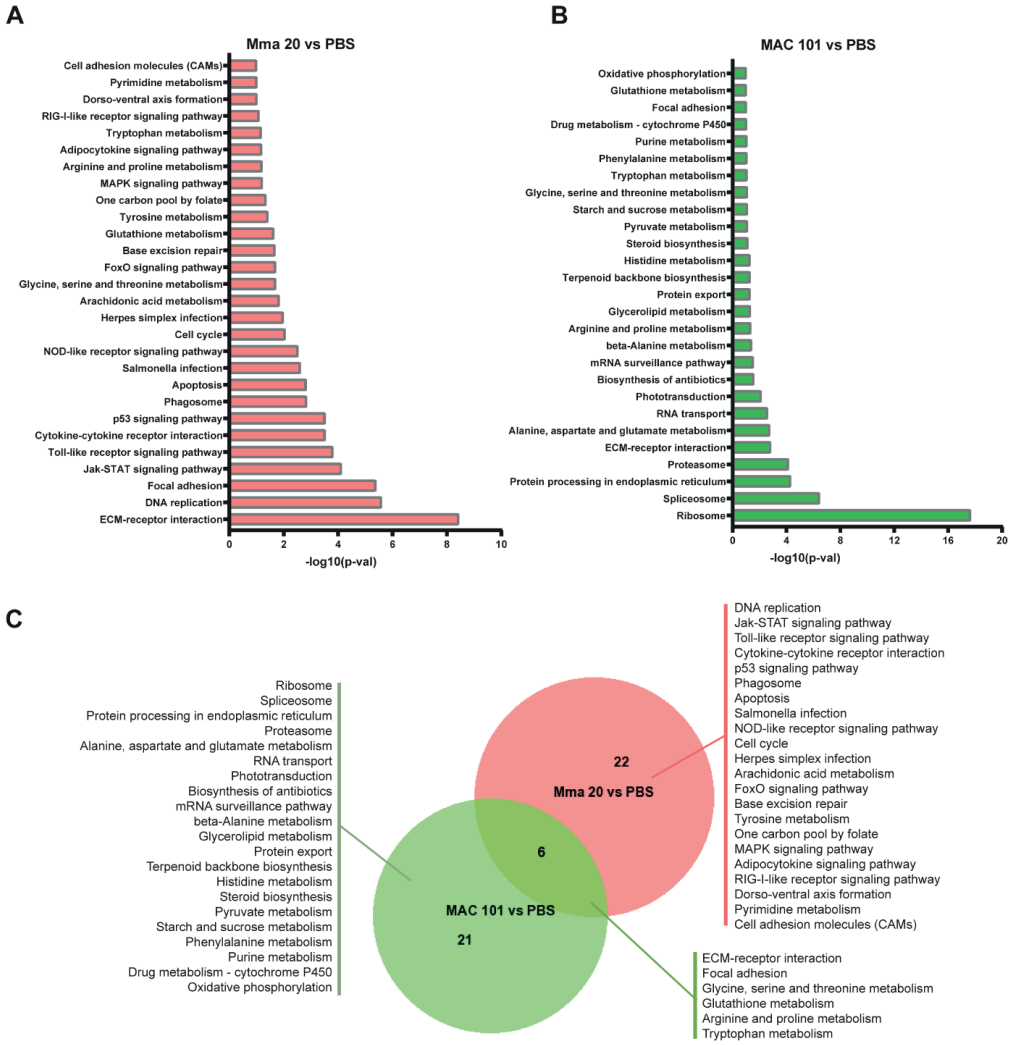

Supplementary figure 1 Significantly enriched KEGG pathways based on DAVID functional analysis. (A) Significantly enriched pathways in zebrafish embryos upon Mma 20 infection. (B) Significantly enriched pathways in zebrafish embryos upon MAC 101 infection. (C) Venn diagram of the enriched KEGG pathways in zebrafish embryos infected with Mma 20 and MAC 101. The comparison was performed on Mma 20 *vs* PBS and MAC 101 *vs* PBS.

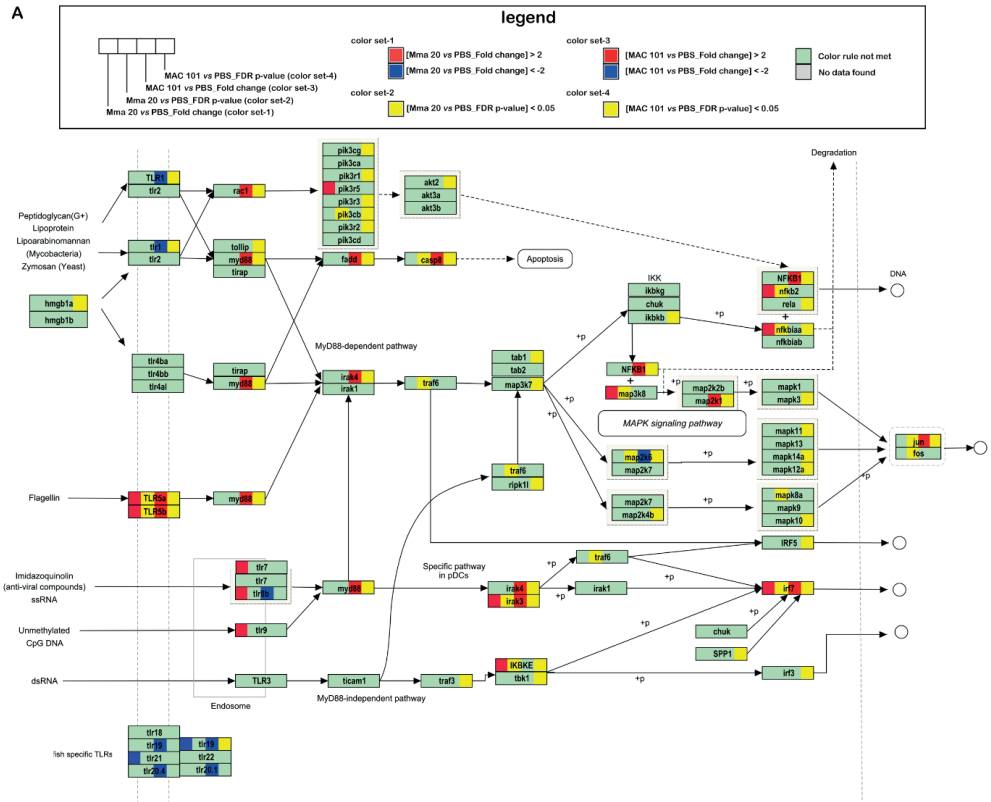

Supplementary figure 2 Toll-like receptor signaling pathway upon *M. marinum* Mma20 or *M. avium* MAC 101 infection. The pathway was adapted from the Wiki pathway. In the visualization, the gene expression in the comparison of Mma20 infection *vs* PBS and MAC 101 infection *vs* PBS are depicted by color (red, upregulated; blue, downregulated; yellow, FDR *p*-value < 0.05).

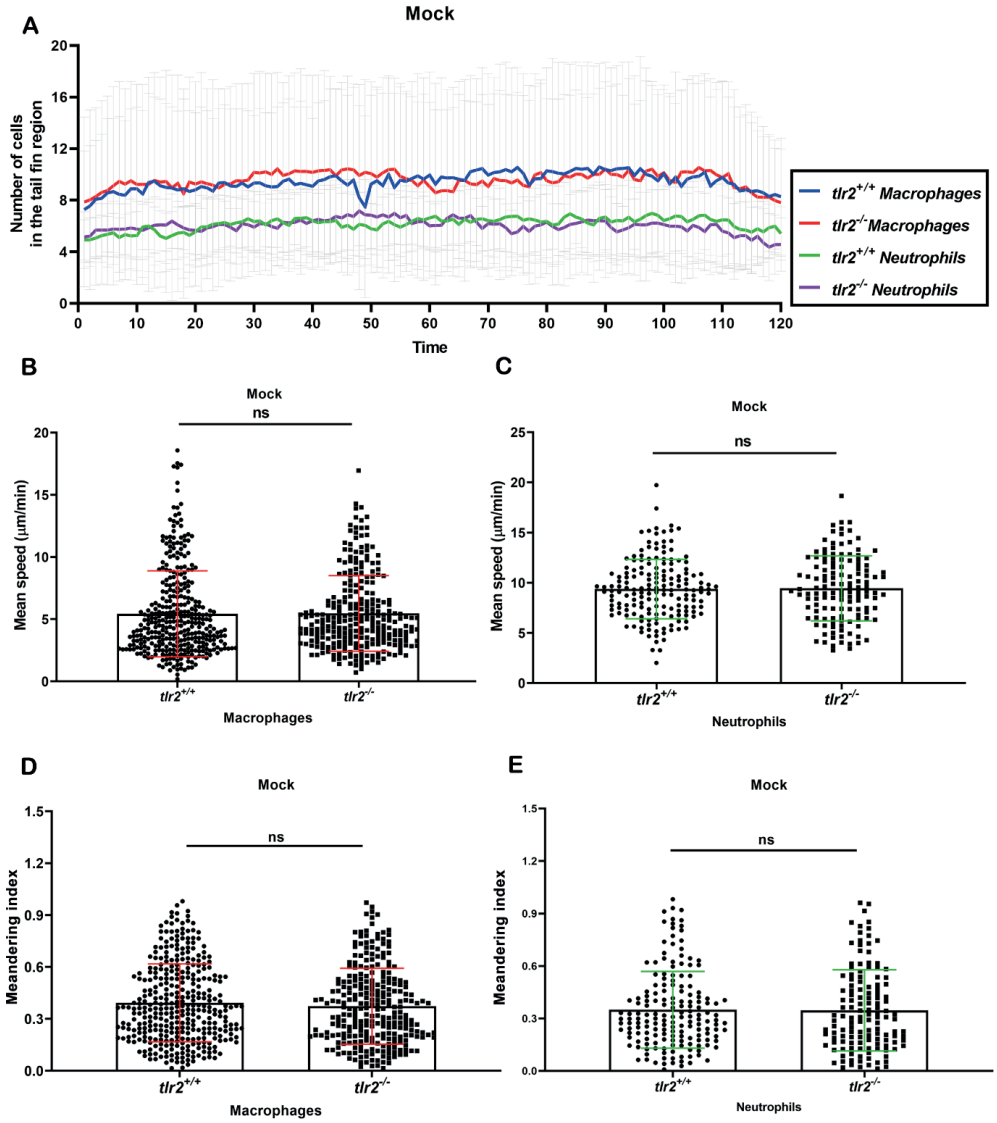

Supplementary figure 3 Quantification of leukocytes behavior in *tlr2* mutant and sibling control larvae after mock injection in tail fin. (A) The number of recruited leukocytes to the tail fin region upon mock infection. (B) The mean speed of tracked macrophages in PBS injected tail fin region. (C) The mean speed of tracked neutrophils in PBS injected tail fin region (D) The meandering index of tracked macrophages in PBS injected tail fin region. (E) The meandering index of tracked neutrophils in PBS injected tail fin region. Data (mean ± SD) were combined from three independent experiments with 5 or 6 fish in $tlr2^{+/+}$ or $tlr2^{-/-}$ group. An unpaired, two-tailed t-test was used to assess significance. ns, non-significant; *, $P < 0.05$, ****, $P < 0.0001$. Scale bar: 100 μm; Sample size (n): 347, 273; 170, 134 (B, D, and C, E).

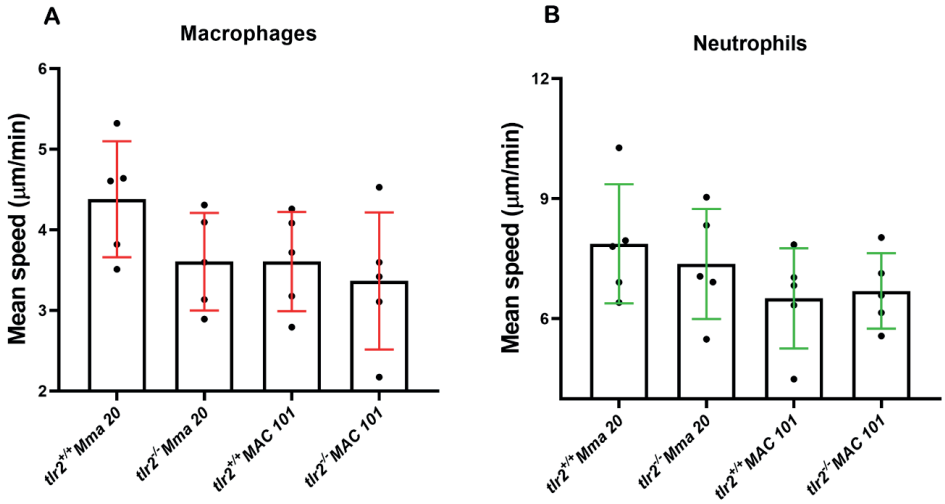

Supplementary figure 4 Quantification of leukocytes overall means speed in *tlr2* mutant and sibling control larvae after *M. marinum* Mma20 or *M. avium* MAC 101 injection in the tail fin. The quantification of the leukocytes overall mean speed was performed by Track Foci plugin. (A) Overall mean speed of macrophages in *tlr2*$^{+/+}$ and *tlr2*$^{-/-}$ zebrafish larvae after Mma 20 or MAC 101 infection. (B) Overall mean speed of neutrophils in *tlr2*$^{+/+}$ and *tlr2*$^{-/-}$ zebrafish larvae after Mma 20 or MAC 101 infection. Each point represents the mean speed of all specific cells from an individual zebrafish.

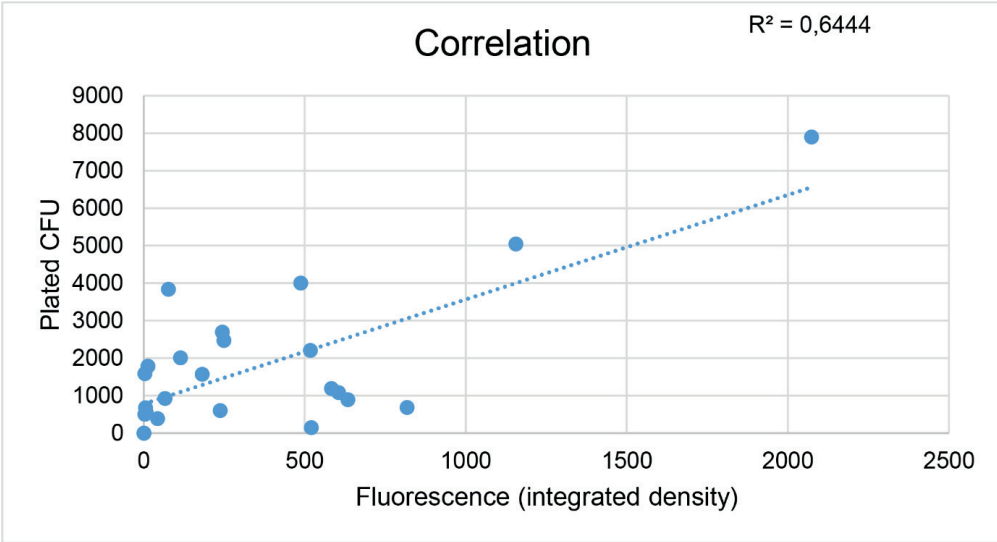

Supplementary figure 5 The correlation between MAC 101 CFU and average fluorescence signal.